Noise Measurements and Analyses of Nanodevices

A Thesis

submitted to
Indian Institute of Science Education and Research Pune
in partial fulfillment of the requirements for the
BS-MS Dual Degree Programme

by

Ninad Salgaonkar

Indian Institute of Science Education and Research Pune
Dr. Homi Bhabha Road,
Pashan, Pune 411008, INDIA.

March, 2026

Supervisor: Atikur Rahman

Certificate

This is to certify that this dissertation entitled ”Noise Measurements and Analyses of Nanodevices” towards the partial fulfilment of the BS-MS dual degree programme at the Indian Institute of Science Education and Research, Pune represents study/work carried out by Ninad Salgaonkar at Indian Institute of Science Education and Research under the supervision of Atikur Rahman, Associate Professor, Department of Physics, during the academic year 2025-2026.

Atikur Rahman

Committee:

Atikur Rahman

Bijay Kumar Agarwalla

This thesis is dedicated to Dr. Ashna Bajpai,
who was kind to me when I needed it the most.

Declaration

I hereby declare that the matter embodied in the report entitled ”Noise Measurements and Analyses of Nanodevices” are the results of the work carried out by me at the Department of Physics, Indian Institute of Science Education and Research, Pune, under the supervision of Dr. Atikur Rahman, and the same has not been submitted elsewhere for any other degree. Whatever others contribute, every effort is made to indicate this clearly, with due reference to the literature and acknowledgement of the collaborative research and discussions.

Ninad Salgaonkar

Acknowledgements

I am indebted to a lot of people without whose help this thesis wouldn't have been possible. Special thanks to Pawan Kumar Gupta, Saqlain Mushtaq and the Sofer group from UCT Prague who grew the crystals and fabricated from them the devices which were measured in this thesis. Also thanks to Pawan Kumar Gupta and Avinash Mahapatra who built the nitrogen bath cryostat in which some of the devices were measured. All the work that I managed to do throughout the year has been possible only because other researchers have spent years working in this field - Dr. Graziella Scandurra, Dr. Carmine Ciofi and Dr. Aveek Bid. Especially thanks to Dr. Scandurra for providing me with a pre-print of her paper that I didn't have access to.

I extend my deepest gratitude to Atikur sir. He has provided me with invaluable guidance throughout the year. His knowledge of physics is immense. Despite his busy schedule, he has always been present enough for me to turn to him when I couldn't solve a problem. I am also thankful for the freedom he granted me throughout the project, letting me choose the direction the project took. I consider myself incredibly fortunate to have been mentored by someone of his caliber. Beyond academic matters, his guidance on personal and professional development has also been invaluable to me.

Also thanks to my TAC member, Dr. Bijay Kumar Agarwalla, who has been incredibly kind. Thanks to Pawan bhaiya, Avinash bhaiya, Sudipta bhaiya and Swapneswar who have been extremely helpful in the lab. Without their consistent support, I would have been lost on my own and unable to do anything. Also thanks to Nilesh sir and other technical staff at IISER Pune, espectially Karthikeyan who has helped me out a lot with electronics and drilling. Thanks to Prabhu bhaiya and Pankaj bhaiya who helped me to vacuum the nitrogen insert when our lab's vacuums were occupied, even at odd hours.

Finally, I am thankful to all the members of the NanoQ lab, including Atikur sir and Ayesha ma'am, for making an incredibly welcoming environment for me. I especially enjoyed my talks about science and academia with Sudipta bhaiya and Sagnik bhaiya. It's because of them that my master's thesis has been through and through a great experience that I am going cherish for my life.

Thank you.

AI Usage Notice

I declare that the use of Generative AI in this thesis did not extend beyond what is described

in Section 4.6.1 of the ‘Guidelines for Generative AI usage at IISER Pune’, and accordingly, no attribution is required.

Abstract

Usually, in transport experiments on 2D materials, mean values of quantities like voltage and current are measured. However, even in steady states, these quantities show fluctuations around their mean values, which is called as noise. Noise presents multiple new statistical quantities that we can measure in order to probe the microscopic processes occurring in the material. Here, we measure the Power Spectral Density of noise, which naturally separates out the processes occurring on different time scales since it is frequency resolved.

Noise power spectral density is usually calculated by measuring the transport quantity at high sampling rates and performing algorithms like Welch's periodogram on the data collected. In such cases, the lowest magnitudes of the noise power spectral density that can be measured is often limited by the power spectral densities of the instruments used for the measurement, usually the preamplifier used for signal conditioning. The cross-correlation technique enables us to measure noise magnitudes below the noise floor of the measuring apparatus by making two simultaneous measurements at once. In this thesis, we implemented a cross correlation setup that can measure voltage noise power spectral density magnitudes as low as 1.6×10^{-19} V^2/Hz, which is below the noise floor of the voltage amplifiers we used.

Next, we probed devices made from 2D materials using noise spectroscopy. We performed temperature-dependent noise spectroscopy measurements on CrSBr in order to determine presence and type of n-type donors. We detected signatures of generation-recombination processes at low temperatures in the form of random telegraph noise whose attempt frequencies had an Arrhenius-type of variation with temperature.

For tellurene, our aim was to detect signatures of presence of phase transitions. So, we performed temperature- and gate voltage-dependent noise spectroscopy. Through temperature dependent measurements, we detected increase of $1/f$ noise exponent at 220K, which could be a signature of critical fluctuations. However, time-domain analysis revealed that fluctuations are due to a very slow random telegraph process whose attempt frequencies were outside our measurement window. This serves to highlight the complexities involved in interpreting noise data. We also present here the data of how the $1/f$ noise magnitude changes with gate voltage at a fixed temperature.

Contents

List of Figures

List of Tables

Chapter 1

Introduction

The main aim of this thesis is use the fluctuations or noise in the electronic transport properties as a probe of 2D materials. The total electronic noise in a 2D material has contributions from many different sources, the most common of which are tabulated in table 1.1.

To differentiate between the various types of noise, the noise power spectral density (PSD) is calculated. Measurements of noise PSD can give information that measurements of mean value alone can't. For example, the noise produced in current due to the discreteness of charge, called shot noise, is given by,

$$S_I(f) = 2e\langle I \rangle$$

...where, e is the quantum of charge. Thus, measurements of shot noise PSD can give the charge on each charge carrier and has been used to confirm the presence of fractional charge carriers in the fractional quantum Hall regime[1, 2].

Consider a voltage time series data of length N where the time interval between each sample is t_s: $v(nt_s)$, where n = 0, 1, 2, ... N-1. The sampling frequency will be, $f_s = \frac{1}{t_s}$. Let the Discrete

Type	Source	Spectra
Johnson-Nyquist	Random thermal motion of electrons	White/Constant
Shot	Discreteness of charge	White/Constant
Flicker	Debated	1/f
Random Telegraph	Generation and recombination of charge carriers	Lorentzian

Table 1.1: Common sources of electronic noise in 2D materials

Fourier Transform (DFT) of this series be defined as,

$$V(f) = \frac{1}{\sqrt{N}} \sum_{n=0}^{N-1} v(nt_s) \exp(-i2\pi f n t_s) \tag{1.1}$$

...where, $f = 0, \frac{f_s}{N}, \frac{2f}{N}, ..., f_s - \frac{f_s}{N}$

Then the inverse Discrete Fourier Transform will be,

$$v(t) = \frac{1}{\sqrt{N}} \sum_{m=0}^{N-1} V\left(\frac{mf_s}{N}\right) \exp\left(i2\pi \frac{mf_s}{N} t\right) \tag{1.2}$$

...where, $t = nt_s$, for some $n \in \{0, 1, 2, ..., N-1\}$.

The inverse DFT is just the time series $v(t)$ written as a linear combination of the Fourier modes given by,

$$P_f(nt_s) = \frac{1}{\sqrt{N}} \exp(i2\pi f n t_s)$$

...where, $f = \frac{mf_s}{N}$, for some $m \in \{0, 1, 2, ..., N-1\}$

They form an orthonormal set.

$$\sum_{n=0}^{N-1} P_f^*(n) P_{f'}(n) = \delta_{ff'}$$

And since they are N many vectors, they form an orthodnormal basis of the space of all time series of length N. This gives a very useful interpretation of the DFT, $V(f)$. It is just the vector $v(t)$ written in the basis of the Fourier modes.

The DFT gives the (complex) coefficient of the Fourier mode with frequency f in this decomposition. This coefficient may also be written as,

$$V(f) = A(f) e^{i\phi(f)}$$

..., where $A(f)$ and $\phi(f)$ are both real and give the amplitude and the starting phase, respectively, of the Fourier mode with frequency f.

$A(f)$ will have units of voltage. Since, for a resistor,

$$\text{Power} = \frac{V^2}{R}$$
$$\therefore \text{Power} \propto V^2$$

So, we define the following quantity as the Power Spectral Density (PSD) of the voltage time series, $v(nt_s)$,

$$S_v(k) = \frac{A(f)^2}{\Delta f} = \frac{|V(f)|^2}{\Delta f}$$

...where, $\Delta f = \frac{f_s}{N}$ is the separation between frequencies. Similarly, we can also measure a time series of current data and calculate its PSD, $S_I(f)$.

If N is even (which will always be the case throughout this thesis), f can be taken to have the values $-\frac{f_s}{2}+\frac{f_s}{N}, -\frac{f_s}{2}+\frac{2f_s}{N}, \ldots \frac{f_s}{2}$, which is the convention that will be used throughout this thesis.

Since voltage and current time series are purely real, their PSDs will always be symmetric, $S(-f) = S(f)$. Exception here is the Nyquist frequency, $f_s/2$, which does not have a negative counterpart. Because a PSD usually looks better on a log-log plot, it is customary to report the one-sided PSD instead of the two-sided PSD as defined above. To construct this, the PSDs calculated at all the negative frequencies are added to their positive counterparts. Thus in a one-sided PSD, all the values are twice of what they would be in a two-sided PSD, except for the Nyquist frequency (which doesn't have a negative counterpart in a two-sided PSD) and the 0 frequency (which is its own negative).

1.1 Random Telegraph Noise

In many semiconductor devices, a special kind of noise is observed. When the device is in a biased state, it is found that the current or the voltage switches at random between two or several discrete values. The time intervals between switchings are random, but the two values of the fluctuating quatities are time-independent.(Chapter 8 of [3]) This type of noise is known as random telegraph noise. Sometimes the random telegraph noise is thermally activated, i.e., it occurs in thermal equilibrium, due to transitions of electrons between two states with well-defined energies that are separated by an potential barrier.[4] In such cases, the spectra created by random telegraph noise is lorentzian,

$$S_{RT} = \frac{A_2 f_C}{f_C^2 + f^2} \tag{1.3}$$

...where, the parameter f_C is called the attempt frequency and follows the Arrhenius equation,

$$f_C = f_{C0} \exp\left(\frac{-E_a}{k_B T}\right)$$

...where, E_a is the activation energy of the two-level fluctuations, i.e., the potential barrier that needs to be surmounted. f_C is interpreted as the frequency at which crossing of the potential barrier is attempted.[3] How the above function looks on a log-log plot is shown in fig. 1.1.

In semiconductors, random telegraph noise usually occurs due to generation-recombination processes. Conduction in semiconductors is mostly done by electrons present in the conduction band, which are delocalized states. Defects or impurities present in the crystal structures introduce localized states in the semiconductors. Electrons in these localized states cannot take part in conduction and so these states are called trap states. When current is flowing through such a

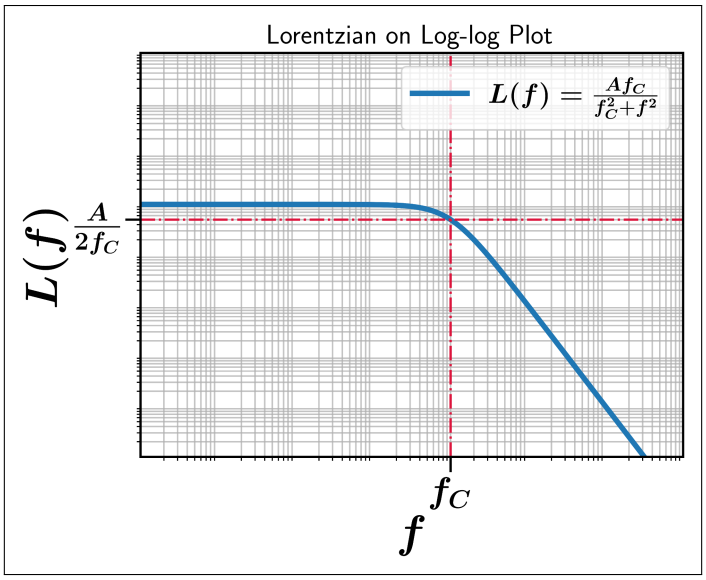

Figure 1.1: Lorentzian function plotted eq. 1.3 on a log-log scale. Values used for the parameters: A_2=2 and f_C=10^{-6}

semiconductor, the process of trapping-detrapping of conduction electrons in these localized states happen continuously. Thus the number of charge carriers fluctuates, leading to random telegraph noise in the voltage or current across the semiconductor.

1.2 $1/f$ noise

$1/f$ noise is also variously known as flicker, pink or excess noise. It's spectra is given by,

$$S(f) = \frac{A_2}{f^{\alpha}}$$

...where, $0.8 \leq \alpha \leq 1.4$ is considered as $1/f$ noise.[5] Thus, $1/f$ noise dominates at low frequencies. $1/f$ noise has been observed in a vast number of semiconductors, semiconductor devices, semimetals, superconductors, metals in normal state, tunnel junctions, etc.[3] All the measurements on samples done in this thesis were carried out in the frequency range where $1/f$ noise dominates.

Of course there are mathematical problems with a $1/f$ spectra. The spectrum diverges at f=0. Also, the integration of a $1/f$ spectrum from 0 to ∞ diverges as well. The integration of Power Spectral Density gives the average power of the time series and so this is unacceptable.[5] It is commonly believed that at low enough frequecies, the PSDs would deviate from an exact $1/f$ behaviour. However, measurements of noise PSDs upto $10^{-6.3}$ Hz (which took several weeks to measure) has shown exact agreement with a $1/f$ form.[6]

There exist some debate on the origins of $1/f$ noise. The most popular model, owing to its

simplicity, on how $1/f$ noise emerges, is McWhorter's.[7] It states that a material exhibiting $1/f$ noise has many different trapping processes within it. Each of these traps contributes a Lorentzian to the noise spectrum with a different attempt time τ_C (inverse of the attempt frequency f_C). If the traps with different attempt times τ_C have a distribution given by,

$$g(\tau_C)\tau_C = \frac{B}{\tau_C} d\tau_C$$

...then, an integration over their GR spectra will give a $1/f$ spectrum,

$$S(f) = \int_0^\infty g(\tau_C) S_{GR}(f) d\tau_C = \int_0^\infty \frac{B}{\tau_C} \cdot \frac{A_2 \tau_C}{1+(\tau_C f)^2} d\tau_C$$

$$S(f) = \frac{BA_2}{f}$$

Why would there be this particular distribution of attempt times? When McWhorter gave this model, he was studying metal-oxide semiconductors. In those devices, the charge carriers are present in the semiconductor, but the traps are present in the thin layer of oxide that has been deposited on them. So the charge carriers need to tunnel through a barrier to the traps. This causes the attempt times to depend exponentially on the distance of the traps from the semiconductor.[7]

$$\tau_C = \tau_{C0} e^{x/\lambda}$$

If we assume a homogenous distribution of trap states in the oxide layer, i.e. $dg/dx = 1$, we get the required distribution of attempt times.[7]

$$\frac{dg}{d\tau_C} = \frac{dg}{dx}\frac{dx}{d\tau_C} = \frac{dg}{dx}\frac{-\lambda}{\tau_C}$$

Thus, $1/f$ noise in metal-oxide semiconductors can arise from very natural assumptions. However, this particular distribution of attempt frequencies needs to be justified for all the vast number of meterials in which $1/f$ noise is observed.

Dutta, Dimon and Horn generalized McWhorter's model.[8, 5] They showed that an approximate $1/f$ spectrum can arise from a broad distribution of trap states over activation energies $D(E_a)$, as long as the distribution varies slowly compared to $k_B T$. They showed that the the frequency exponent in a $1/f$ spectrum and the temperature dependences of noise are correlated.

$$\alpha(f,T) = 1 - \frac{1}{\ln(2\pi\omega\tau_0)} \left(\frac{\partial \ln S_V(T)}{\partial \ln T} - 1 \right)$$

....where, τ_0 is the characteristic attempt time, which DDH had assumed to be of the order of inverse phonon frequency for metals. This equation can be used to verify whether the Dutta-Horn model applies to a given material or not. If it does, the model gives a way to calculate the distribution of trap states as a function of energy.

$$D(E_a) \propto \frac{f}{k_B T} S_V(\omega, T)$$

The Dutta-Horn model has been found to be applicable, for example, in the case of Ag metal strips.[9]

The kinds of models discussed above are called number fluctuation models, because they attribute the origin of the $1/f$ noise to fluctuations in the number of charge carriers. There are others who instead advocate for mobility fluctuation models, the most prominent of whom is F.N. Hooge.[7] Voltage or current fluctuations are also caused due to scattering of charge carriers off of phonons or defects in the crystal lattice. Proponents of these models argue that $1/f$ noise emerges out of these scattering events. F.N. Hooge attributes $1/f$ noise to the scattering of the electrons off of phonons.[10] Optical scattering experiments have shown that intensity of acoustic lattice modes vary with a 1/f spectrum.[11] There is also some data, for example, of Hall coefficient measurements in n-GaAs, which suggests that $1/f$ in this material originates due to carrier mobility fluctuations rather that carrier number fluctuations.[12]

Finally, $1/f$ noise has also been observed outside of electronic systems, for example, in current fluctuations in biological ion channels[13], DNA sequences[14], volatility of stock market prices[15], etc. This creates a want for a more general mechanism for the origin of $1/f$ noise

1.3 Noise near electronic phase transitions

Near 2nd order electronic phase transitions, it is seen that the total noise shows a diverging increase, the $1/f^{\alpha}$ noise exponent increases significantly above 1, autocorrelation time of the time series data increases and it acquires non-Gaussian characteristics. These are just the manifestations of the universal features of second order phase transitions - critical opalescence, critical slowing down and divergence of correlation length.[16, 17]

At a 1st order electronic phase transitions, where among the two coexisting phases, one is insulating and the other is conducting, large random telegraphic noise is seen in the transport properties. This happens because the domains of the two phases are constantly fluctuating from one to another.[18]

Chapter 2

Noise spectroscopy setup

2.1 Hardware

We can either measure the voltage noise or the current noise of a device under test (DUT). If Z_D is the small signal equivalent impedance of the DUT at any given DC bias, then the voltage and current noise PSDs are related by,[19]

$$S_V = |Z_D|^2 S_I$$

Generally, voltage noise measurements are preferred for DUTs with low resistances and current noise measurements are preferred for DUTs with high resistances.[19]

The schematic used to measure voltage noise is shown in fig. 2.1a and the schematic to measure current noise is shown in fig. 2.1b. To measure voltage noise, a constant current source was used to bias the DUT and the voltage across the DUT was amplified using a home-built amplifier built according to the design in [20]. The voltage signal was then filtered by an anti-aliasing low-pass filter and then digitized using the MCC USB-1808X simultaneous-sampling Data Acquisition (DAQ) Card. For the current source, a 12V lead acid battery along with a ballast resistance of a value much larger than the DUT's resistance was used. Batteries are preferred because they have less noise of their own compared to power supplies or source meter units.

To measure current noise, the DUT was biased using a constant voltage source, which was a 12V battery whose voltage was reduced using a voltage divider. The current flowing across the DUT was converted into a proportional voltage signal using the DL Instruments Model 1211 current preamplifier and then filtered and digitzed same as above.

According to the Shannon-Nyquist sampling theorem, if the PSD of continuous-time signal is calculated by sampling it at a frequency of f_s, then the PSD can be accurately constructed only if the frequency content of the signal has a bandwidth of at most f_s. If the PSD of the signal is non-zero over a wider range, we'll run into the problem of 'aliasing', i.e., power from two frequencies will be added to the same frequency bin in the PSD. So, it's necessary to limit the bandwidth of

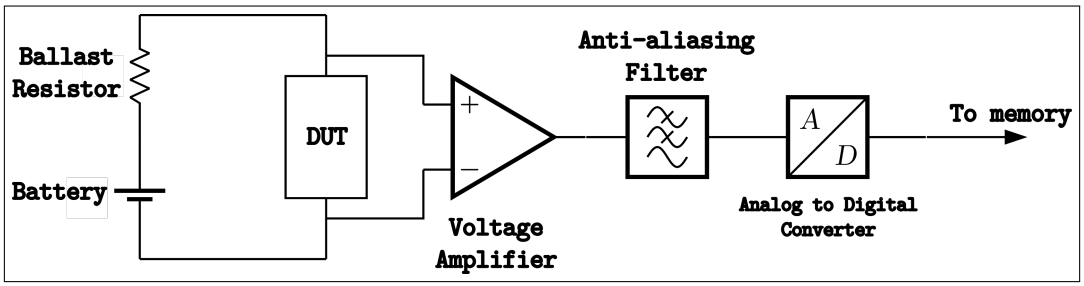

(a) Voltage Noise Measurement Circuit

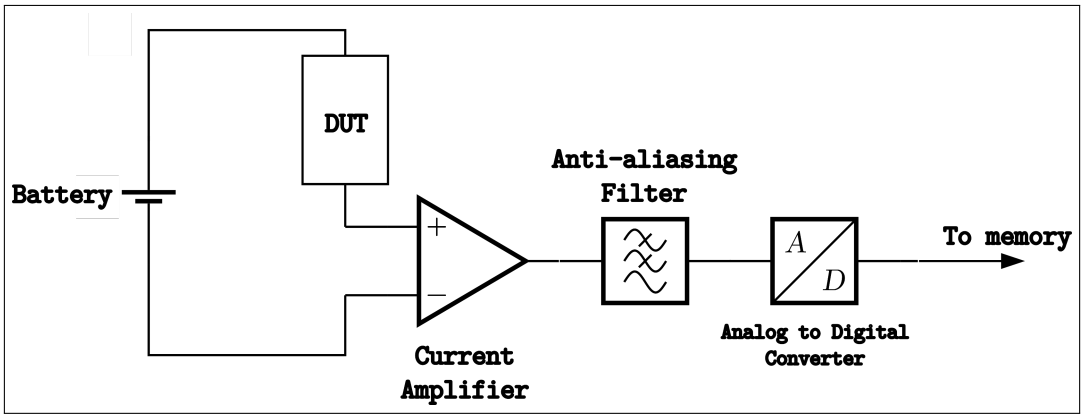

(b) Current Noise Measurement Circuit

Figure 2.1: Circuits used for Noise Measurements

(a) RC Filters (b) Active Filters

Figure 2.2: Antialiasing Filters

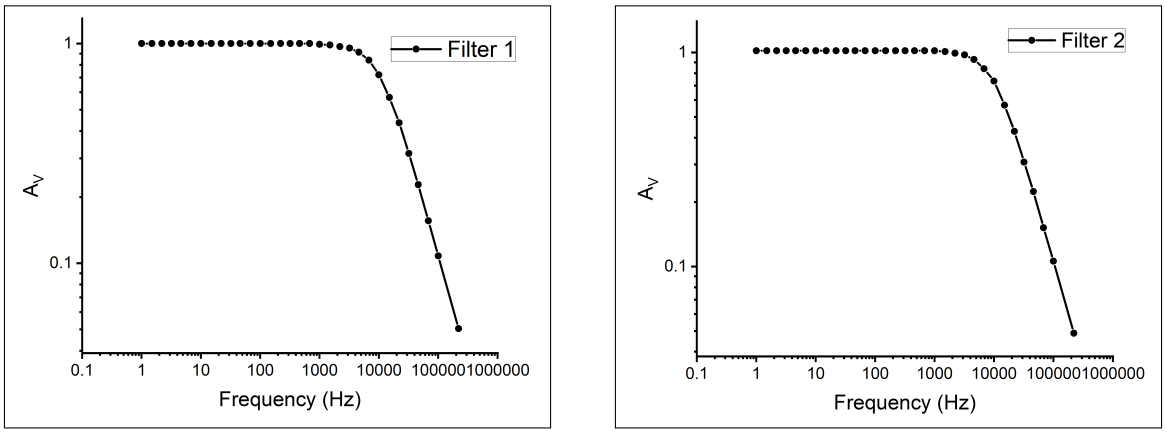

Figure 2.3: Frequency response of RC filters with cutoff at ≈15 kHz

the signal before it's sampled by the DAQ card, which we achieve by placing low-pass filters just before it.

First, we made RC filters with a cutoff-frequency of ≈15 kHz. Their frequency responses were measured by inputing a sinusoidal wave of a particular frequency and amplitude V_{in} using a Keysight 33600A waveform generator, and measuring the amplitude, V_{out}, of the output sinusoid using an oscilloscope. Then,

$$A_V = \frac{V_{out}}{V_{in}}$$

The frequency responses are plotted in fig. 2.3. We were unsatisfied with their roll-offs and so built 4th order active filters, two with cutoff frequencies at 300 Hz and one with cutoff frequency at 30 kHz. The filters had two Sallen-Key stages and designed to have Butterworth frequency response. The schematic circuits of the active filters is shown in fig. 2.4. Their frequency responses, measured in the same way as for RC filters, are plotted in fig. 2.5 and 2.6. For the 300 Hz filter, the frequency response drops by more than 40 dB, i.e, more than 100 times, by 1000 Hz. So, a sampling rate of 2000 Hz or above is sufficient to prevent the problem of aliasing. Similarly, frequency response of 30 kHz filter drops by more than 100 times by 100 kHz and so sampling rate of 200 kHz is sufficient.

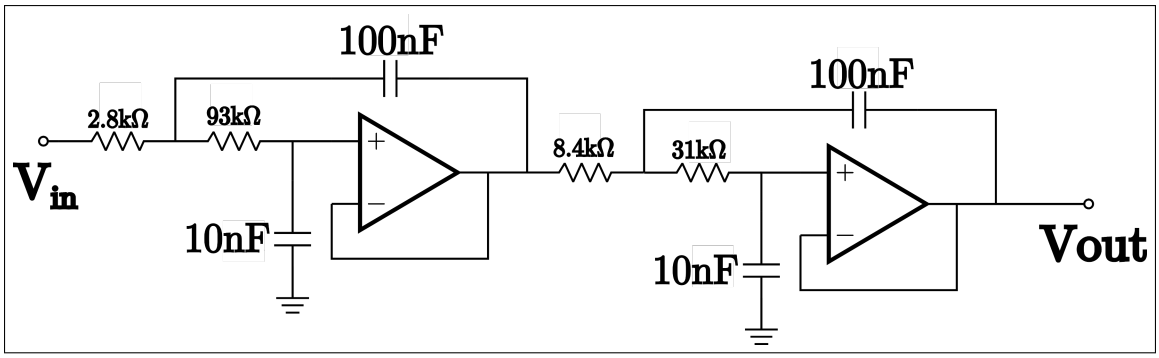

(a) Cutoff frequency = 300 Hz

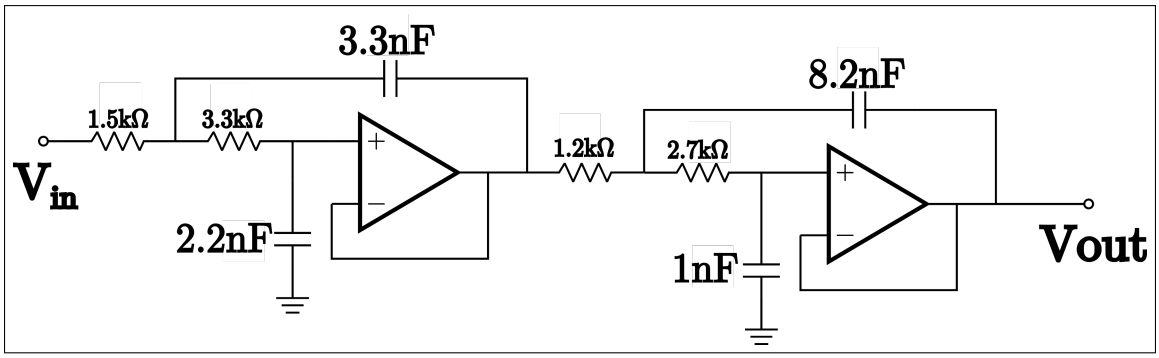

(b) Cutoff frequency = 30 kHz

Figure 2.4: Schematic of the anti-aliasing filter circuits. The op-amp used for this circuit was LT1169 dual op-amp.

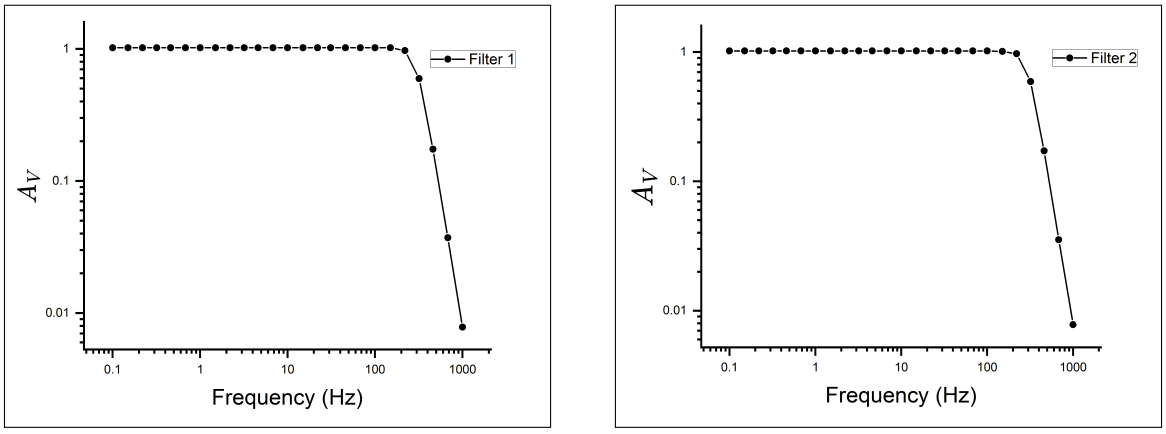

Figure 2.5: Frequency response of active filters with cutoff at 300 Hz

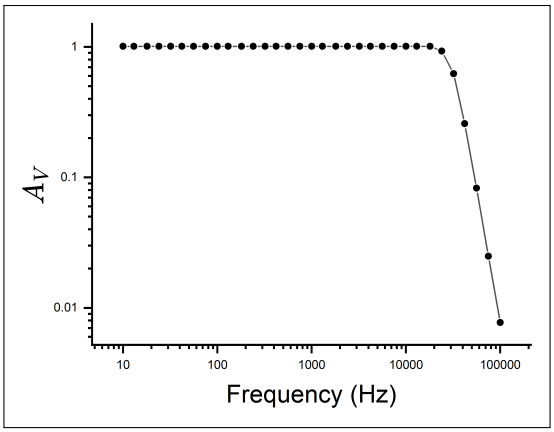

Figure 2.6: Frequency response of active filter with cutoff at 30 kHz

The RC filters were used for the measurements mentioned in this chapter. However, for all measurements on actual samples mentioned in Chapters 3 and 4, active filters with cutoff frequency of 300 Hz and a sampling rate of 2048 Hz were used.

2.1.1 Low temperature measurements

Temperature-dependent noise measurements were performed in either a liquid nitrogen bath cryostat or a closed cycle cryostat. We could continuously control the temperature of devices loaded in both the cryostat using heaters controlled by a LakeShore 350 temperature controller and a LakeShore 335 temperature controller, respectively. Prior to measurements, both cryostats were vacuumed, first by either a scroll or rotatry pump, and then a turbomolecular pump.

2.2 Software

PSD is calculated from the voltage time series data according to the method in [19]. Briefly, a $M \times N$ samples long time series is divided into M many parts of length N. For the hth part, $v_h(nt_s)$, its DFT is calculated as,

$$v_{sm,h}(f) = \sum_{n=0}^{N-1} v_h(nt_s) w(n) \exp(-i2\pi f n t_s) \tag{2.1}$$

$w(n)$ is a window function which is a filter which reduces spectral leakage, i.e., addition of power from neighbouring frequencies to the PSD calculated at a particular frequency. A clearer explanation of how this works is in section 2.2.1.

The best estimate for the PSD is taken as,

$$S(f) = \frac{1}{M \cdot enbw(w)} \sum_{h=1}^{M} |v_{sm,h}(f)|^2$$

...where, $enbw(w)$ replaces Δf. The Equivalent Noise Bandwidth (ENBW) is a quantity that can be calculated for a given window function.

The lowest magnitudes of a PSD that can be measured using the above method is limited by the noise floor of the measuring apparatus, usually the preamplifier used for signal conditioning. The cross-correlation technique[21] can enable us to measure even lower noise magnitudes by making two simultaneous measurements of the voltage across the DUT. These two measurements, however, need to be made separately using two measuring apparatus so that the excess noise in the two measurement channels is uncorrelated. In our case, we used two different amplifiers, two different filters and two different input channels on the simultaneous-sampling DAQ card. DFT is performed on both time series data separately and then they are combined in the following way to get an estimate of the PSD,

$$S(f) = \frac{1}{M \cdot enbw(w)} \sum_{h=1}^{M} \mathfrak{Re}\left\{v^*_{sm1,h}(f) v_{sm2,h}(f)\right\} \tag{2.2}$$

...where, $\mathfrak{Re}\{x\}$ is defined as the function which returns the real part of a complex number x.

We wrote a MATLAB code implementing this algorithm. It is given in lst. 2.1. The Hanning window used in this code is given by,

$$w(n) = \frac{2}{N} \sin^2\left(\frac{\pi n}{N}\right)$$

The factor of $2/N$ is there to make sure the passband of the filter has an amplification of 1. We used this filter because it gives the lowest relative estimation error in a variety of circumstances.[22]

Listing 2.1: Cross-correlation PSD code employing the Hanning Filter.

```
datalogfile='raw.csv';
psdfile='psd.csv';

N=8192;
rate=2048;
M=200;
res=rate/N;

data=readtimetable(datalogfile);



%Creating a Hanning Window
w=(sin(pi*(0:N-1)/N))'.^2;
```

```
[h,f]=freqz(w,1,1,rate);
w=w/h(1);
bw=enbw(w, rate);



%Calculate PSD
psd=zeros(N, 1);

for i=1:M
    v_sm1=fft(data.Board0_Ai0((i-1)*N+1:i*N,1).*w);
    v_sm2=fft(data.Board0_Ai1((i-1)*N+1:i*N,1).*w);
    psd=psd+real(conj(v_sm2).*v_sm1);
end

psd=psd/(bw*M);
psd(2:N/2)=psd(2:N/2)+flip(psd(N/2+2:end));
psd=psd(1:N/2+1);



%Write PSD to file
frequency=(0:rate/N:rate/2)';
writematrix([frequency psd], psdfile);
```

The ref. [23] describes a modification of the above algorithm that uses an IIR filter instead of an FIR filter like Hanning window. An Infinite Impulse Response (IIR) filter is such that it's window function is infinitely long. Now, it's not possible to use an infinitely long window function as that would require infinite calculations. However, a mathematical trick called autoregression or feedback makes it possible to calculate the output of an IIR filter in finitely many steps.

IIR filters have the advantage over Finite Impulse Response (FIR) filters that they have much faster roll-off. A disadvantage of the IIR filters is that they introduce a phase change in each element of the DFT that is frequency-dependent in a non-linear fashion. However, since we are only interested in the absolute value of the DFT, this doesn't affect us.

We implemented an algorithm that uses an 8th order Butterworth filter (an IIR filter) cascaded by a rectangle window filter in a MATLAB code. It's given in lst. 2.2.

Listing 2.2: Cross-correlation PSD code employing an 8th order Butterworth filter cascaded by rectangle window filter.

```
datalogfile='raw.csv';
psdfile='psd.csv';

res=1;
```

```
N=8192
rate=2048;
M=100;
res=rate/N;
ts=1/rate;

data=readtimetable(datalogfile);



%Make an 8th order low-pass Butterworth filter.
wc=pi*res;
num=wc^ord;
den=conv([1 wc*0.390181 wc^2],[1 wc*1.111140 wc^2]);
den=conv(den,[1 wc*1.662939 wc^2]);
den=conv(den,[1 wc*1.961571 wc^2]);
[r,p,k]=residue(num,den);
bw=1.0065*res;



%Calculate PSD.
%Create impulse response vector
w=zeros(N,ord);
for l=1:ord
    w(:,l)=(r(l)*exp((N:-1:1)*p(l)*ts))';
end

%Preallocate variables
psd=zeros(N,1);
vw1=zeros(N,ord);
vw2=zeros(N,ord);
vsm1=zeros(N,ord);
vsm2=zeros(N,ord);
vsmr1=zeros(N,ord);
vsmr2=zeros(N,ord);


%Filter data and calculate PSD
for i=1:M
    v1=data.Board0_Ai0((i-1)*N+1:i*N,1);
    v2=data.Board0_Ai1((i-1)*N+1:i*N,1);

    v1fft=fft(v1);
    v2fft=fft(v2);
```

```
    for l=1:ord
        vw1(:,l)=ts*fft(v1.*w(:,l));
        vw2(:,l)=ts*fft(v2.*w(:,l));

        vsmr1(:,l)=((exp(p(l)*N*ts)-1)*vsm1(:,l)+...
        vw1(:,l)-r(l)*ts*v1fft)/(p(l)*N*ts);
        vsmr2(:,l)=((exp(p(l)*N*ts)-1)*vsm2(:,l)+...
        vw2(:,l)-r(l)*ts*v2fft)/(p(l)*N*ts);

        vsm1(:,l)=exp(p(l)*N*ts)*vsm1(:,l)+vw1(:,l);
        vsm2(:,l)=exp(p(l)*N*ts)*vsm2(:,l)+vw2(:,l);
    end

    psd=psd+real(conj(sum(vsmr1,2)).*sum(vsmr2,2));
end

psd=psd/(bw*M);
psd(2:N/2)=psd(2:N/2)+flip(psd(N/2+2:N));
psd=psd(1:N/2+1);



%Write the PSD to a file.
frequency=(0:rate/N:rate/2)';
writematrix([frequency psd], psdfile);
```

2.2.1 Why cross-correlation works?

In this section, we try to answer why the window function $w(n)$ is used and why cross-correlation manages to go below the noise floor of the measuring apparatus. The answers to these questions are more intuitive if we consider the filter bank interpretation of a Fourier Transform. This discussion is mostly taken from [19].

Consider the inverse DFT, eq. 1. If we multiply both sides by $\exp(-i2\pi r f_s t/N)$,

$$\begin{aligned} v(t)\exp\left(-i2\pi\frac{rf_s}{N}t\right) &= \sum_{m=0}^{N-1} V\left(\frac{mf_s}{N}\right)\exp\left(i2\pi\frac{(m-r)f_s}{N}t\right) \\ &= \sum_{q=-r}^{N-1-r} V\left(\frac{(q+r)f_s}{N}\right)\exp\left(i2\pi\frac{qf_s}{N}t\right) \end{aligned}$$

Now, consider the $q = -r$ term,

$$V\left(\frac{(-r+r)f_s}{N}\right)\exp\left(i2\pi\frac{-rf_s}{N}t\right)$$
$$= \exp\left(i2\pi\frac{Nf_s}{N}t\right)V\left(\frac{(-r+r)f_s}{N}\right)\exp\left(i2\pi\frac{-rf_s}{N}t\right)\exp\left(i2\pi\frac{Nf_s}{N}t\right)$$
$$= V\left(\frac{((N-r)+r)f_s}{N}\right)\exp\left(i2\pi\frac{(N-r)f_s}{N}t\right)$$

...where, we have used the fact that, for some n= 0, 1, 2, ..., $N-1$,

$$\exp\left(i2\pi\frac{Nf_s}{N}t\right) = \exp\left(i2\pi f_s n t_s\right) = \exp\left(i2\pi n\right) = 1$$

Thus, we can replace the $q = -r$ term in the summation above with a $q = N-r$ term. Similarly, we can replace q = $-r+1$, $-r+2$, ..., -1 terms in the summation above with q = $N-r+1$, $N-r+2$, ..., $N-1$ terms. We'll then have,

$$v(t)\exp\left(-i2\pi\frac{rf_s}{N}t\right) = \sum_{q=0}^{N-1} V\left(\frac{(q+r)f_s}{N}\right)\exp\left(i2\pi\frac{qf_s}{N}t\right)$$

Thus, the DFT of the LHS above is just the DFT of $v(t)$ shifted to the left by rf_s/N. So the DFT component of v(t) at frequency of rf_s/N gets shifted to the frequency of 0. If we wanted to calculate that component, we could apply a digital lowpass filter on $v(t)\exp(-i2\pi rf_s t/N)$. We do this by convoluting the time series with another series $l(n)$. $l(n)$ should have a DFT which is 1 from -$\Delta f/2$ Hz to $\Delta f/2$ Hz and zero everywhere else. Since convolution in time domain becomes multiplication in frequency domain, we will get the DFT component at zero frequency.

$$V\left(\frac{rf_s}{N}, g\right) = \sum_{n=0}^{N-1} v(nt_s)\exp\left(-i2\pi\frac{rf_s}{N}t\right)l(g-n) \tag{2.3}$$

...where, we have assumed periodic boundary conditions for $l(n)$, i.e., that $l(n+N) = l(n)$.

Finally, if we do the substitution $l(g-n) = w(n)$, i.e., take the window function as just the reverse of the filter's convolutional kernel,

$$V\left(\frac{rf_s}{N}\right) = \sum_{n=0}^{N-1} v(nt_s)w(n)\exp\left(-i2\pi\frac{rf_s}{N}t\right)$$

...we realize that this is just the DFT as defined in eq. 2.1. Thus, we realize that a DFT is just a filter bank, i.e., a collection of bandpass filters that filter out different frequencies from a time series data to give the entire spectrum.

Note that we get an estimate of $V(rf_s/N)$ for every g in eq. 2.3. However, we only use one of them as otherwise we are calculating multiple estimates from the same data point and the error in that data point adds up.

Finally, we can square $V(f)$ obtained above to get the power and divide it by Δf to get the power spectral density. However, the filter $l(n)$ I described above with the "brickwall" frequency response is idealized and does not exist. One of the non-idealities that real filters have is that away from the passband, they don't go to zero directly. Instead they only asymptotically go to zero. So, a lot more power passes through them than necessary.

To account for this non-ideality, we replace Δf in the definition of PSD by the Equivalent Noise Bandwidth of the window function, $w(n)$. enbw(w) is defined as the width of the passband of the brickwall filter whose area under its frequency response is the same as the area under $w(n)$'s frequency response.

Finally, suppose that instead of single channel measurements, we make two measurements. Both the measurements have the signal, $V(f)$, coming from the DUT. But each channel also adds channel-specific noise $\delta V_1(f)$ and $\delta V_2(f)$. These noise may have the same statistical characteristics, but they are uncorrelated with each other and with $V(f)$. So if we multiply both and take their average,

$$\begin{aligned}\langle (V+\delta V_1)(V+\delta V_2)\rangle &= \langle V^2\rangle + \langle V\delta V_1\rangle + \langle V\delta V_2\rangle + \langle \delta V_1 \delta V_2\rangle \\ &= \langle V^2\rangle + \langle V\rangle\langle \delta V_1\rangle + \langle V\rangle\langle \delta V_2\rangle + \langle \delta V_1\rangle\langle \delta V_2\rangle \\ &= \langle V^2\rangle\end{aligned}$$

...if the mean of the channel specific noise is zero. This is how we isolate the signal coming only from the DUT.

2.3 Validation of the Cross-correlation method

To verify that the cross-correlation setup that we have implemented works, we used it to measure the voltage noise across unbiased metal film resistors. At equilibrium, the voltage across the leads of a resistor shows fluctuations around zero due to the random thermal motion of electrons. This is known as Johnson-Nyquist noise. The magnitude of these fluctuations is related to the resistance of the resistor by the fluctuation-dissipation relation. If $S_V(f)$ is the one-sided voltage noise PSD,

$$S_V(f) = 4k_BTR \tag{2.4}$$

Voltage across the resistor was sampled at a rate of 200 kHz and was collected for 1000 s using two separate measurement channels. We used a value of 200000 for N, i.e., calculated spectra with resolution of 1 Hz and averaged over 1000 such spectra. We used data from only one channel to calculate a single channel PSD and also calculated a cross-correlation PSD using the code employing the FIR filter/Hanning window. The results of PSDs determined from single and two channel measurements are plotted in fig. 2.7. The horizontal straight lines represent what the magnitude of the PSDs ought to be according to eq. 2.4. We measured noise at ambient temperature and used 300 K while calculating the expected noise magnitudes.

Single channel measurements are not being able to accurately determine the noise levels of the 100 Ω and 10 Ω resistances. The excess noise from the instruments causes the PSDs to be at higher

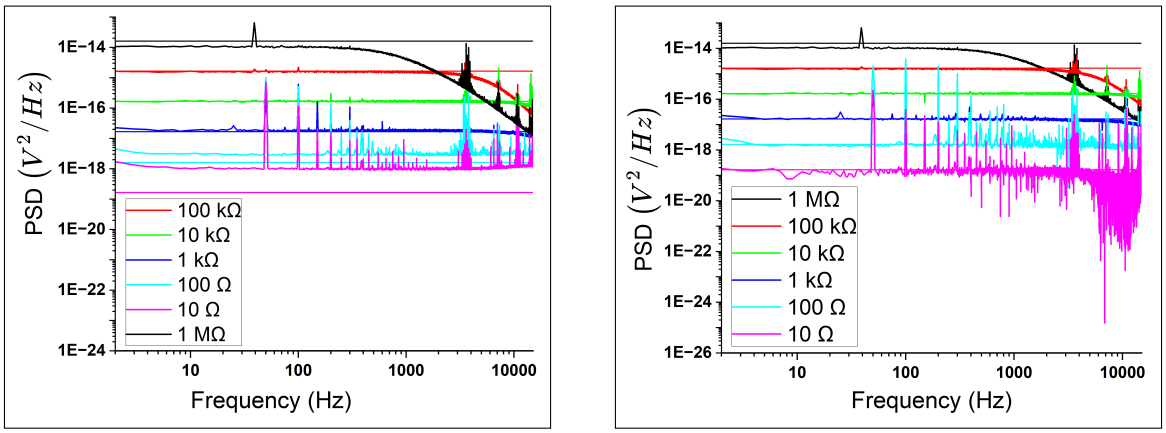

(a) Using single channel measurements

(b) Using cross-correlation

Figure 2.7: Measured PSDs of unbiased metal-film resistors. The solid lines represent the magnitude predicted by the Fluctuation-Dissipation relation

values than expected. On the other hand, cross-correlation measurements are able to determine the noise magnitudes of both 100 Ω and 10 Ω resistances correctly.

In both measurements, however, the calculated PSD of the noise across 1 MΩ resistor is lower than expected. We believe this is due to input resistance loading effect. The input impedance of an amplifier is supposed to be much higher than the resistance which it is amplifying the voltage across of. If that is not the case, then an appreciable amount of current flows through the input terminals of the amplifier as well and so the voltage that it "sees" across the resistor decreases. The amplification then gets reduced. (Chapter 2 of [24]) Thus, our amplifiers' input impedance might be comparable to 1 MΩ. This then sets a limit of 100 kΩ as the maximum resistance of the sample that we can perform noise measurements on.

There are also peaks present in the data at frequencies which are multiples of 50 Hz. We believe this is 50 Hz contamination from surrounding electronics which we are not being able to get rid of completely. Note that the resistor was kept in an aluminium box, the amplfiers and filters are also made in aluminium boxes and the DAQ card was also kept inside a metal box, all of which were grounded.

We also measured additional resistance below 100 Ω using cross-correlation for further verification. Calculated PSDs are plotted in fig. 2.8, and show good agreement with eq. 2.4.

We also reanalyzed the data collected above using the code that employs an IIR filter. The results are shown in fig. 2.9. The PSDs are almost exactly the same, except for low resistances at low frequencies, the PSDs deviate from being completely flat. For this reason, all the PSDs in the following chapters were calculated using the FIR filter algorithm.

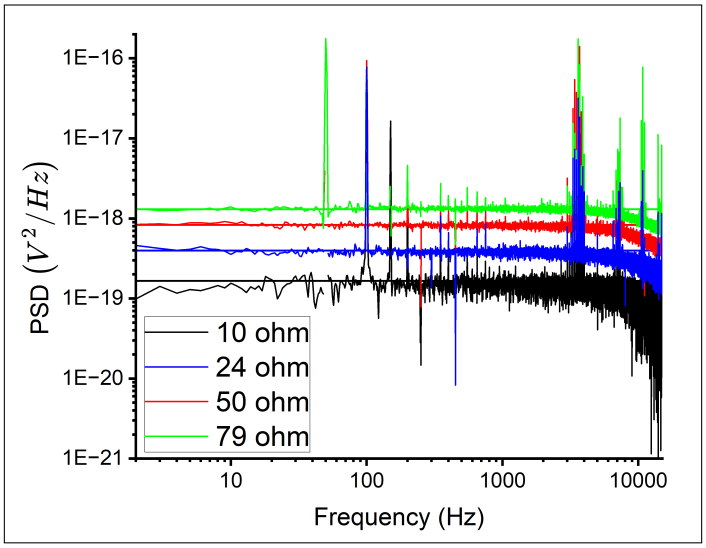

Figure 2.8: Measured PSDs of unbiased metal-film resistors with resistances below 100Ω. The solid lines represent the magnitude predicted by the Fluctuation-Dissipation relation.

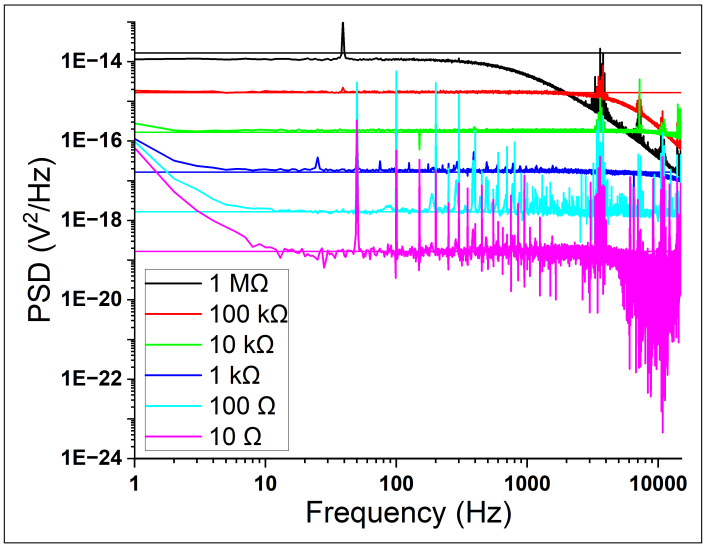

Figure 2.9: Measured PSDs of unbiased metal-film resistors calculated using the algorithm that uses an IIR filter. The solid lines represent the magnitude predicted by the Fluctuation-Dissipation relation.

Chapter 3

Characterization of defect states in CrSBr

CrSBr is a 2D semiconductor with a direct bandgap of 1.5-2 eV. Its crystal structure is shown in fig. 3.1a. ARPES measurements on bulk, undoped CrSBr crystals at room temperature have revealed conduction band filling, which suggests that some unintentional defect may be present which leads to n-type doping.[25] Previously, this doping was attributed to bromine vacancies (V_{Br}) due to similar number densities.[26] Bromine vacancies have been widely observed in vapor-grown CrSBr and believed to be the defects with the highest concentration.[27, 28] However, recent work that employs Density Functional Theory calculations suggests that chromium interstitials (Cr_i) stabilized between CrSBr layers is the most favourable electron donor in terms of having the lowest formation energy in wide range of growth conditions. XPS data suggests that Cr interstitials may also be present in CrSBr samples.[25]

To determine what defects may be present in CrSBr and if they may be causing n-type doping, we decided to perform temperature-dependent current noise spectrscopy on them. Noise spectrscopy has been used before to characterize energetics of defect states.[33, 4] We performed measurements on vapor-grown CrSBr samples that were provided to us by the Sofer group from UCT Prague. The synthesis process of the CrSBr crystals is described here [34]. Saqlain Mushtaq of our fabricated the CrSBr device D2 on an SiO_2 substrate. The Raman spectroscopy he did to confirm the presence of CrSBr crystals is plotted in fig. 3.1b. Pd-Au contacts were made on the sample across its A axis. Measurements were done in a 2 probe configuration.

First we measured the IV characteristics of the device at room temperature, which is plotted in fig. 3.2a. The resistance of the sample is of the order of MΩ. We also measured the temperature-dependence of the resistance of the device. For this, we loaded the device in the nitrogen bath cryostat and measured the current of device at different temperatures on applying a bias of 100 mV. The results are plotted in fig. 3.2b. This data is noisy and hard to draw inferences from. However, it does clearly show that the resistance only increases with decreasing temperature.

Owing to the high resistance of this device, current noise PSD measurements are preferred. We first measured the current noise PSD across the sample when no bias voltage is applied, which is shown in fig. 3.3. This gives the total magnitude of the equilibrium noise of the DUT and the noise

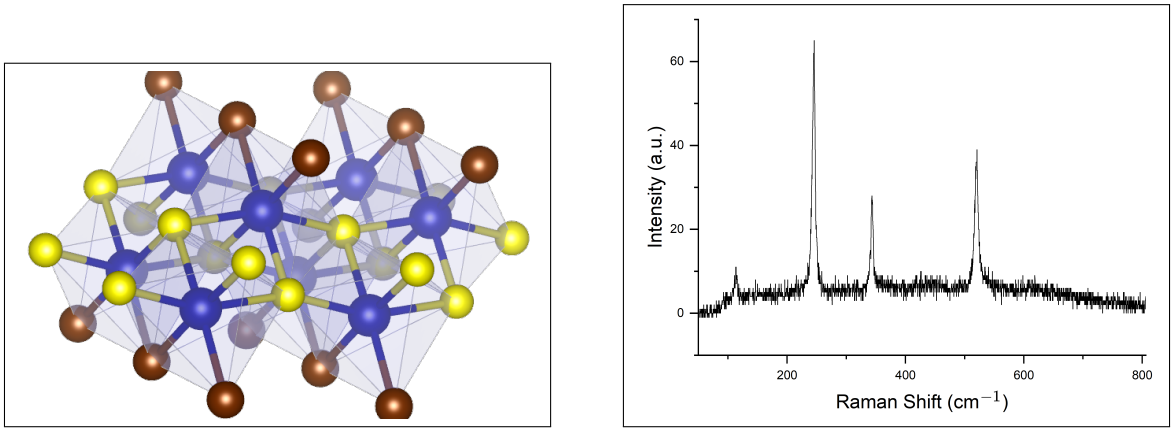

(a) (b)

Figure 3.1: (a) Crystal structure of CrSBr.[29, 30, 31, 32] The blue atoms are Cr, yellow are S and brown are Br. (b) Raman spectroscopy of CrSBr crystals.

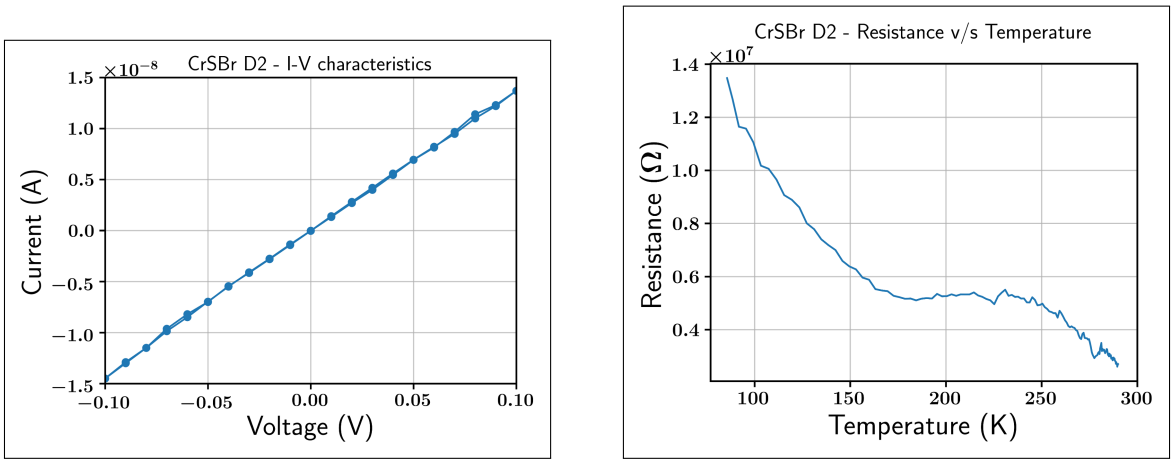

(a) (b)

Figure 3.2: (a) I-V characteristics of CrSBr D2. (b) Resistance vs Temperature plot of CrSBr D2.

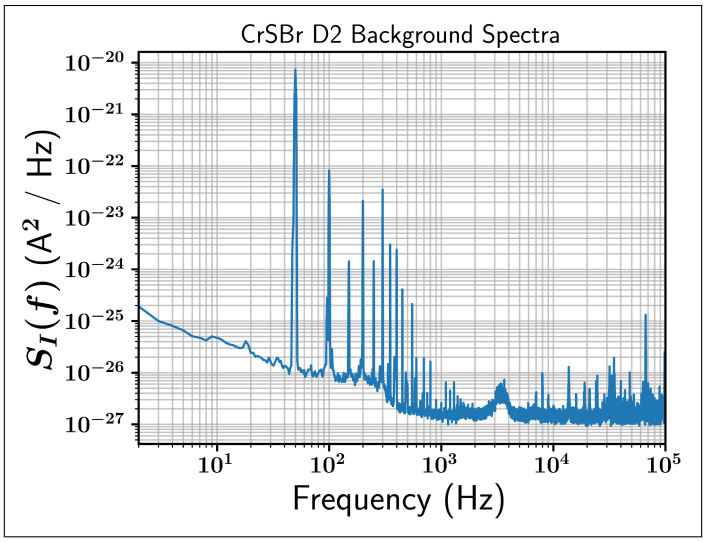

Figure 3.3: Current Noise PSD of unbiased CrSBr D2.

floor of the measuring instruments. The spectra we measure later all have magnitudes orders of magnitude larger than this (fig. 3.4b).

We applied a bias voltage of 0.12 mV and sampled the current through the device. We filtered the current time series digitally using a notch filter that cuts out the contributions from frequencies which are multiples of 50 Hz. Some of the current traces are plotted in fig. 3.4a. We can observe random telegraph noise in them. Note that by RTN, we mean the sudden increases or decreases in the current magnitude that happen stochastically with time. There is also a periodic component with 100 cycles in the 2s long time traces we have plotted. We believe that these are 50 Hz contaminations that, although reduced by digital filtering, still haven't been eliminated completely.

From the unfiltered time series data, we calculated the PSDs of the current noise at the temperatures where random telegraph noise was present. The spectra are plotted in 3.4b. As can be seen, the spectra are not straight lines on a log-log plot and so are not purely $1/f$. We believe that there are also Lorentzian contributions present in the spectra. If true, then the attempt frequency parameter of the Lorentzians f_C seems to be increasing with temperature, as would be the case for a thermally activated process.

We fit the noise spectra at each temperature to the following equation, which has a $1/f$ term and a Lorentzian term corresponding to the Generation-Recombination noise.[4]

$$S_I(f) = \frac{A_1}{f} + \frac{A_2 f_C}{f_C^2 + f^2} \tag{3.1}$$

Note that in this fitting and from the plots 3.4b and 3.5a, we have manually dropped the datapoints of the PSDs calculated at multiples of 50 Hz and one frequency above and below, as they prevented proper fitting. We attribute these peaks to the 50 Hz contamination from apparatus' and surrounding electronics and we don't expect them to correspond to any physical process in the DUT itself.

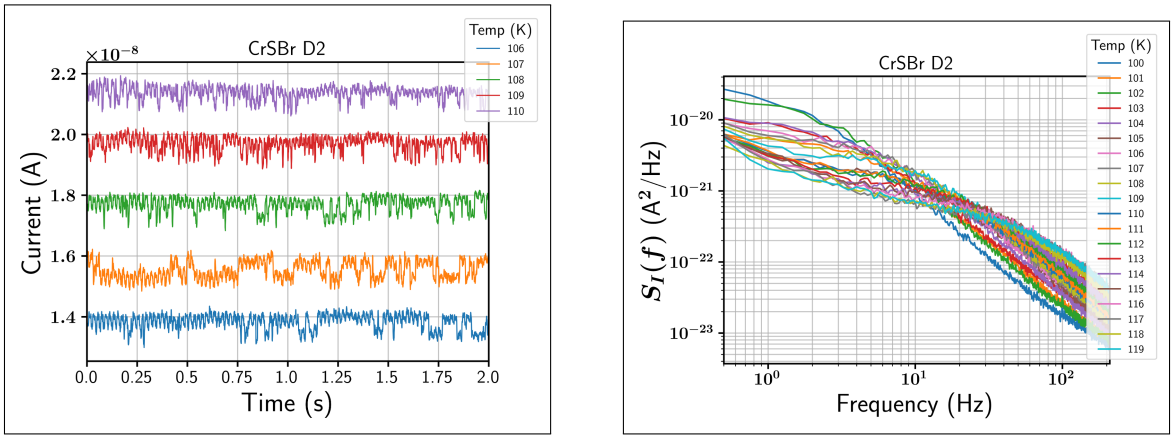

(a) (b)

Figure 3.4: (a) Filtered current time traces across CrSBr D2 at different temperatures. The traces are offset in the vertical direction for clarity. The Y-axis scale is just to indicate the magnitude of the fluctuations. (b) Current noise PSDs of a CrSBr device in the temperature range where it shows Random Telegraph noise.

When the spectrum is $1/f$, the error in the estimated PSD at the different frequencies depend on those frequencies. If the frequencies are kf_s/N, where k goes from 0 to $N/2$, then the relative estimation error at the different frequencies for $1/f$ are given by,[22]

$$\mathrm{REE}(k) = k \ln\left(\frac{2k+1}{2k-1}\right) - 1$$

The fitting of the spectra was done in Python using optimize.curve_fit function of the SciPy library. The above REE was passed to the function as relative errors in the determined PSDs. The fitting to the PSDs at some of the temperatures is shown in fig. 3.5a. In this plot, the frequency times the PSDs is plotted on the Y axis. If the spectra had been purely $1/f$, the graphs would have been flat. The peaks in these graphs are thus due to the Lorentzian components.

Through the fitting, we obtained the values of the fitted parameter f_C from the spectra at different temperatures. The values of $\log(f_C)$ vs $1/T$ are plotted in fig. 3.5b. They show an approximately linear trend which confirms that the two-level fluctuations that give rise to the Lorentzian noise is in fact thermally activated. From the slope obtained by a linear fit to the data, we can get the activation energy E_a,

$$E_a = k_B \times \text{slope} = 140 \pm 1.2 \text{ meV}$$

Density Functional Theory calculations suggest that charge transmission levels of potential electron donors lie in the band gap of CrSBr. The potential donors are bromine vacancies (V_{Br}), chromium interstitials (Cr_i) and Bromine-on-Sulphur antisites (Br_S), i.e., when a position which is usually occupied by a sulphur atom is occupied by a bromine atom. Among these, Cr_i and Br_S are

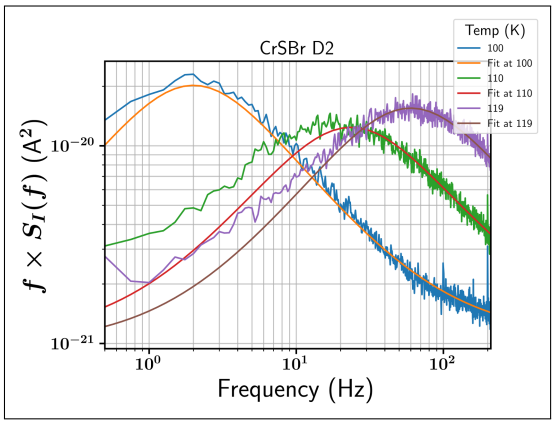

(a) The frequency times PSD plots and their corresponding fits at some temperatures.

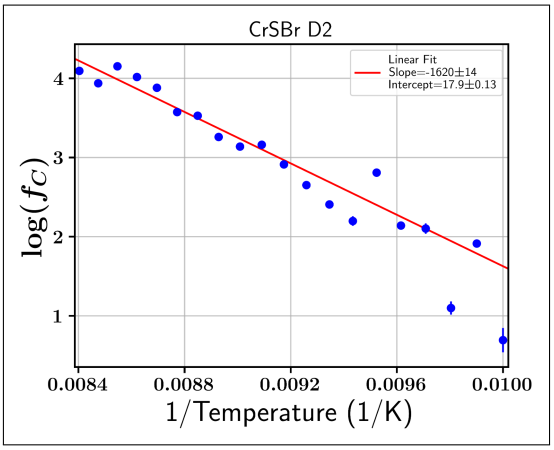

(b) $\log(f_C)$ vs $1/T$ plot and the corresponding linear fit.

Figure 3.5: Determination of activation energy of the two-level fluctuations in CrSBr D2.

predicted to be relatively shallow donors and V_{Br} is predicted to be a relatively deep donor.[25] If these defects are present in our samples, they may be the cause behind the Lorentzian component seen in our noise spectra.

At low temperatures, the electrons are localized to the impurities. When temperature is increased and k_BT becomes comparable to the energy separation between the energy of the trap state and the conduction band minimum (which in our case is 140 ± 1.2 meV), the electrons start getting excited to the conduction band and relaxing back to the trap state, leading to generation-recombination noise. At high enough temperatures, an electron will have equal probability of being in the trap or conduction state and hence we'll have n-type doping at room temperature.

Thus, the Lorentzian noise we observed might be a signature of n-type doping in our samples. Of course there are many other sources of random telegraph noise and so we need corroborating evidence, either from other experiments or density funcitonal theory calculations to be sure of this and to determine exactly which type of defect is responsible.

We tried to repeat the measurements on a different CrSBr device, D3. However in the current time traces of this device, shown in fig. 3.6, we couldn't see any clear random telegraph noise.

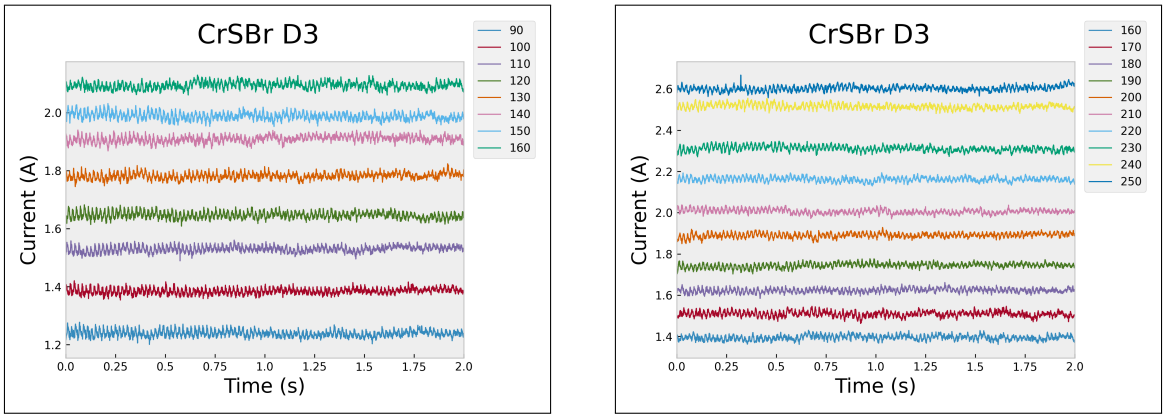

Figure 3.6: Filtered current time traces across CrSBr D3 at different temperatures. The traces are offset in the vertical direction for clarity. The Y-axis scale is just to indicate the magnitude of the fluctuations.

Chapter 4

Temperature- and Gate Voltage-dependent Noise in Tellurene

Gate-tuned metal insulator transitions (MIT) are observed in a large number of 2D materials.[35, 36, 37] A p-type semiconductor is said to be exhibiting an MIT if at large positive gate voltages, its resistance decreases with temperature (insulator-like behaviour) and at small or negative voltages, its resistance increases with temperature (metal-like behaviour); and vice versa for n-type semiconductors. The exact reason behind these transitions are debated with some people favouring different explanations for different materials. Possible mechanisms suggested are that these transitions may be band-tuned, disorder-driven, interaction-driven[38] or percolation-driven[36].

Gate voltage controls the Fermi level and so by changing the gate voltage you can control whether the Fermi level lies within a band or in a band gap. This is the band-tuned transition between metal-like (Fermi level within a band) and insulator-like (Fermi level in band gap) states.[38] Changing gate voltage also changes the carrier density in the material which can lead to interaction-driven phase transitions like Mott-Wigner transitions.[36] Anderson has shown that strong enough disorder can also localize all electronic states within a band. Such localization works better in a low carrier density systems, meaning we could potentially tune such localization using gate voltage.[39] Disorders can also introduce spatial fluctuations in the potential that the electrons face. If these fluctuations in potential are smooth enough, we can have percolation transition. As you increase the gate voltage, first the locations where the potential has minima fill up with conduction band electrons. As long as these conducting domains do not form a contiguous area from one end of the material to another, the material behaves like an insulator. As you keep increasing the gate voltage, these domains get bigger and link up, leading to metal-like behaviour.[39]

Tellurene is the name given to nm thick tellurium flakes. In tellurene, atoms covalently bond to form a 1D helical chain. Multiple such chains bonded sideways due to van der Waals interaction make up one layer of tellurium (fig. 4.1). Electrolyte-gated tellurene has been shown to undergo a gate-tuned metal-insulator transition.[40]

Electrolyte gating is a technique to apply gate voltage where the gate contact is made a little

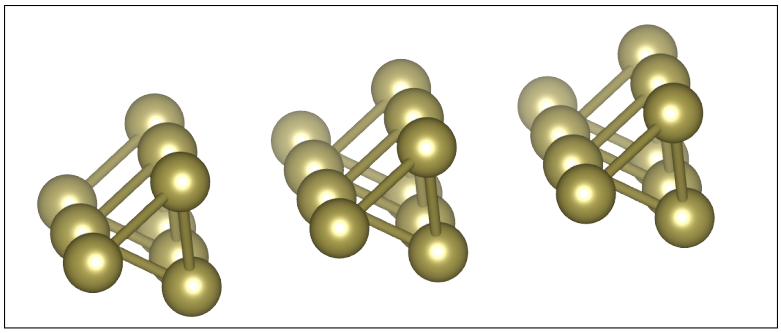

Figure 4.1: Crystal structure of Tellurene.[41, 42, 30, 31, 32]

distance away from the device on the substrate and both are immersed in an electrolytic solution. When a gate voltage is applied, the electrolytes with the charge of opposite sign accumulate near the gate contact and those with same sign accumulate near the device. Because these electrolytes are free ions in a liquid, they are able to bunch up really close to the device and so the electric field that they are able to induce in the device is very high. Correspondingly, electrolyte gating can increase the carrier density of the device to higher magnitudes than the usual metal contact back gating can[43] and can induce metal-insulator transitions in materials that otherwise don't undergo one.[40]

In work lead by Pawan Gupta of our lab, gate-tuned metal insulator transition was observed in a tellurene device that had a typical back gating using a metal contact on the other side of the SiO_2 substrate. The data also showed some interesting temperature-tuned features which we wished to investigate further. However, the reason behind this transition is still not well elucidated. So, we decided to perform noise spectroscopy on tellurene. Since, noise shows characteristic features near second order phase transitions, if we see similar features in our experiments, we could rule out band-tuning or disorder alone as the cause behind the metal-insulator transition in tellurene as both of them are not true phase transitions.

Growth of tellurene crystals and fabrication of tellurene devices D5 and D6 were done by Pawan Gupta. The X-Ray Diffraction and Raman Spectroscopy data collected by him to show proper growth is shown in fig. 4.2b. Growth of tellurium crystals using hydrothermal synthesis is described here [44]. The tellurene devices were fabricated on a SiO_2 substrate and two platinum contacts were made across their C axis. We loaded the devices in the closed cycle cryostat for measurements.

4.1 Temperature-dependent measurements

We first measured the IV characteristics of Te D5 in vacuum at room temperature (fig. 4.3a). The resistance was 15 kΩ. So we can measure voltage noise PSD of this device using our setup. We measured the voltage noise PSD of this device at different temperatures to get the total magnitude of equilibrium noise of the device and noise floor of the measuring apparatus (fig. 4.3b).

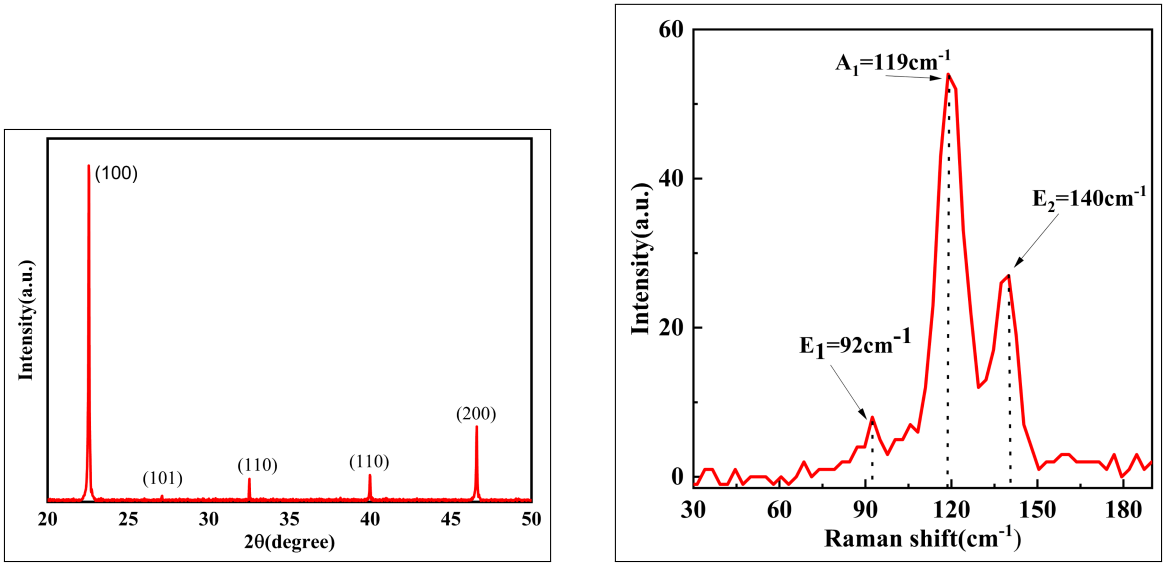

(a) X-Ray Diffraction Pattern

(b) Raman Spectrum

Figure 4.2: Characterization of Tellurene crystals.

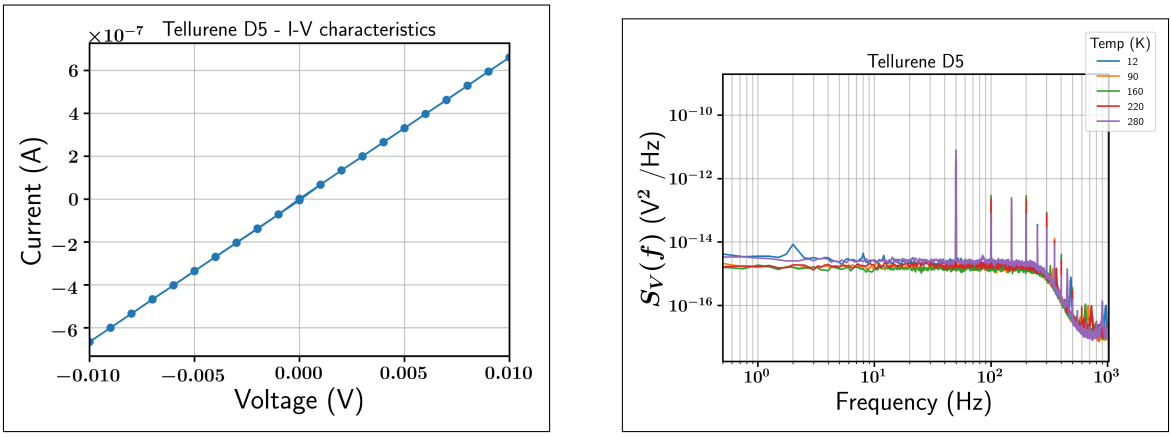

Figure 4.3: (a) I-V characteristics of Tellurene D5. (b) Current Noise PSD of unbiased Tellurene D5 at different temperatures.

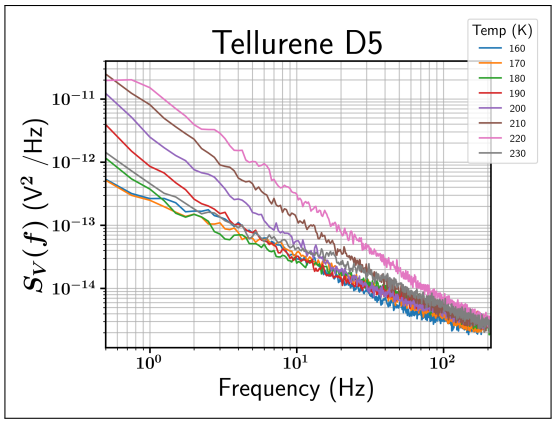

Figure 4.4: Voltage noise PSD of Tellurene D5 shows deviation from an usual $1/f$ noise exponent at 220 K

Temperature	Slope	Error in slope
160	-1.015	0.0081
170	-0.969	0.0058
180	-0.848	0.0063
190	-0.95	0.012
200	-1.25	0.013
210	-1.534	0.0094
220	-1.656	0.0063
230	-0.935	0.0063

Table 4.1: Slopes of the voltage PSDs of Tellurene D5 at different temperatures.

Applying a bias current of 12 μA, we measured the voltage PSD of the device at different temperatures. We observed that the exponent α of the $1/f^{\alpha}$ noise becomes much higher than 1 at 220K. We fitted a line to the $\log(S_V(f))$ vs $\log(f)$ data at some temperaures around 220K. The values of slopes obtained at different temperatures are in table 4.1. Note that these fit parameters were determined without taking into account the errors in the determined PSDs themselves and so the errors in the slopes are probably underestimated.

We wondered if these might be signatures of a second order phase transiton. Note that the resistance vs gate voltage vs temperature data gives no indication of any phase transition at this temperature. To get more insight on this noise feature, we looked at the voltage time traces (fig. 4.5a). We can see that random telegraph noise is present at the temperatures where α is high. The time intervals between the 'jumps' in the data are of the order of seconds. Since the frequency resolution of our calculated PSD was 0.25 Hz, we reasoned that maybe the deviations of α above 1 in our data are due to presence of Lorentzians whose attempt frequencies are below our measurement bandwidth.

We tried fitting the PSDs at temperatures 190-220 K to eq. 3.1. We only got a good fit for the PSD at 220 K (fig. 4.5b), perhaps because it is only at this temperature that the attempt frequency

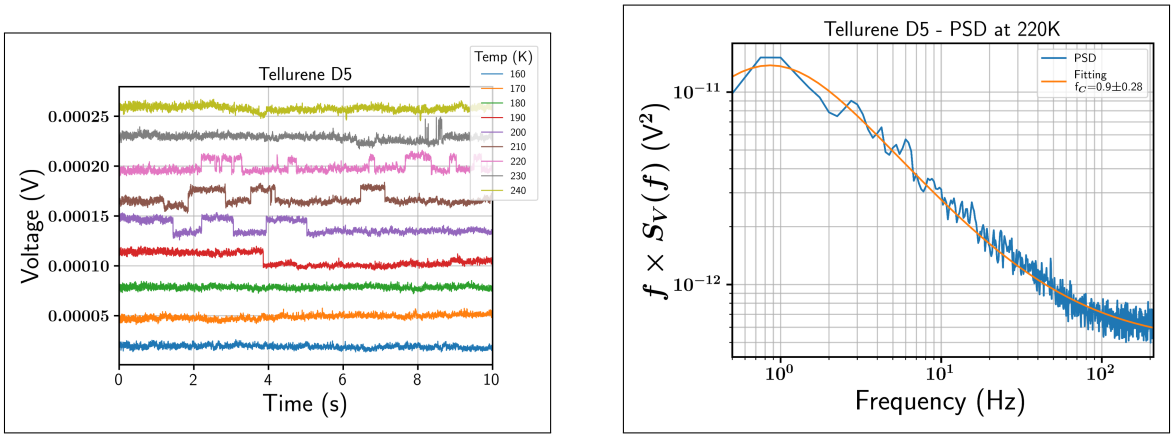

(a) (b)

Figure 4.5: (a) Voltage time series of Tellurene D5 at and around temperatures where spectra shows a deviation from $\alpha = 1$. The traces are offset in the vertical direction for clarity. The Y-axis scale is just to indicate the magnitude of the fluctuations. (b) Fitting of the PSD at 220K to a $1/f$ + Lorentzian function.

is greater than 0.25 Hz, which is the resolution of the calculated PSDs.

From the voltage traces in fig. 4.5a, it appears that the attempt frequencies of the random telegraph noise also increases with temperature. This suggested that maybe the process behind this noise is thermally activated. To probe this process, we decided to perform noise measurements at smaller temperature intervals in the range 196-225 K. The time traces of these measurements are plotted in fig. 4.6. Although we see random telegraph noise in these traces at some odd temperatures, we do not see the expected temperature dependences of the attempt frequencies of these telegraph noises. Furthermore, we do not observe random telegraph noise at the temperatures that we previously observed it at.

We perfomed Resistance v/s Temperature measurements on the device before and after noise measurements; plotted in fig. 4.7. A change in the nature of the tellurene device is apparent. Before the noise measurements, the resistance of the device monotonically decreases with decreasing temperature, showing a metal-like behaviour over the entire measured range of temperature. After noise measurements, the Resistance vs Temperature curve has a minima. Thus, the device shows a metal-like behaviour at high temperatures and a semiconductor-like behaviour at low temperatures. Such a change in nature is usually a sign of degradation of the device. This may be the reason why we didn't observe random telegraph noise in the second temperature sweep.

4.2 Gate voltage-dependent measurements

Since the metal-insulator transition is gate-tuned and not temperature-tuned, if it's a phase transition, it most likely is a quantum phase transition. Strictly speaking, quantum phase transitions

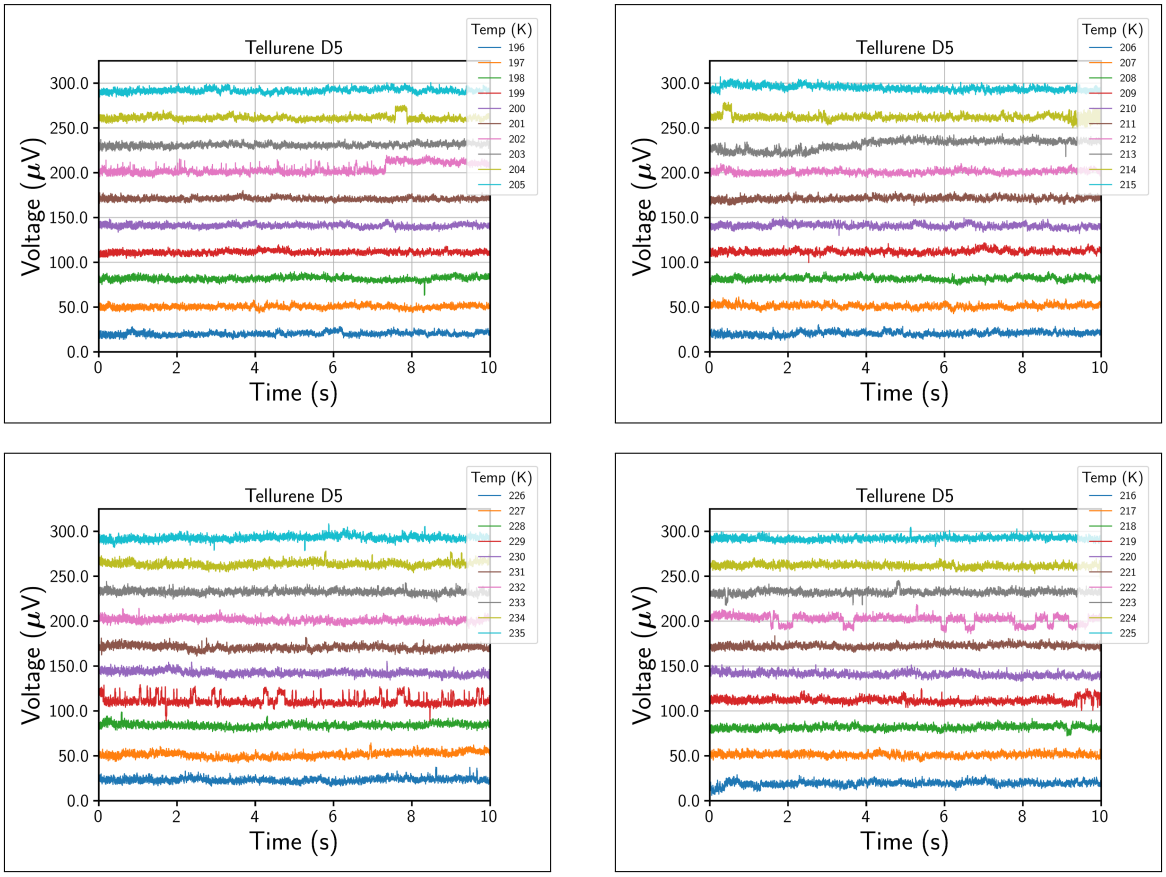

Figure 4.6: Voltage time series data of Tellurene D5 during the second temperature sweep. The traces are offset in the vertical direction for clarity. The Y-axis scale is just to indicate the magnitude of the fluctuations.

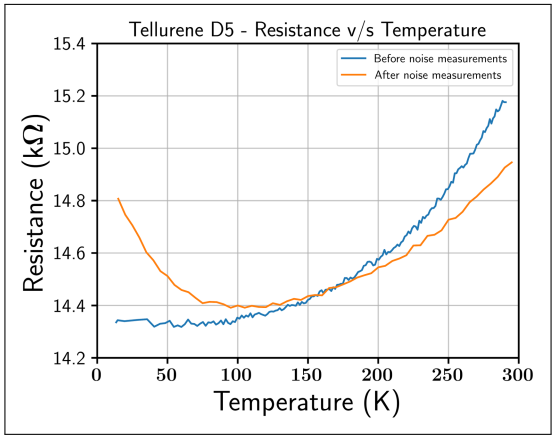

Figure 4.7: Resistance vs Temperature readings of Tellurene D5 taken before and after noise measurements

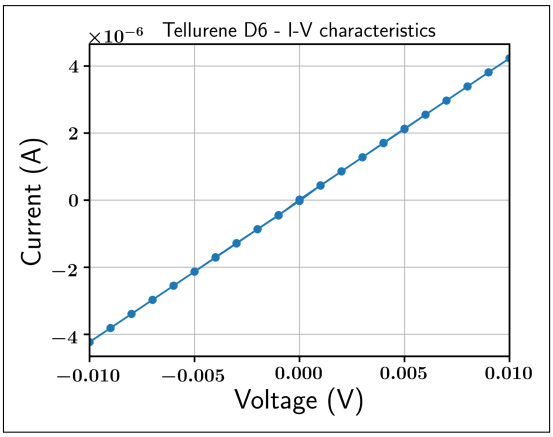

(a) Current v/s Source-Drain voltage.

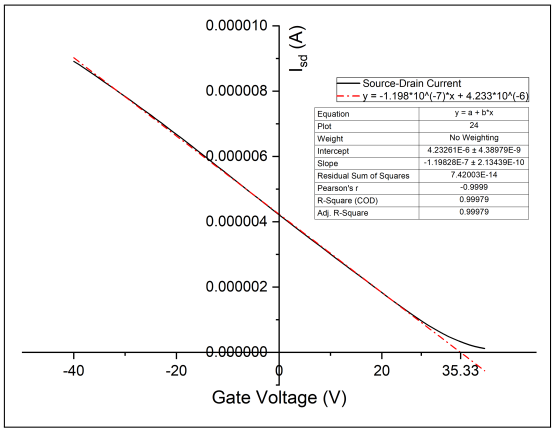

(b) Current v/s Gate voltage

Figure 4.8: Electrical characterization of Tellurene D6.

occur only at 0 K. So its necessary to perform measurements at as low of a temperature as possible to be able to detect signatures of one. We decided to perform noise measurements at 25 K. IV measurement at 25 K (fig. 4.8a) showed that the resistance of Te D6 is ≈2.4 kΩ.

Tellurene is a p-type semiconductor. A scaling collapse analysis on data acquired on another tellurene device showed that the critical gate voltage at which the transition occured was ≈20 V. We performed gate voltage dependent current measurements at a source-drain bias of 0.01 V on the device at temperatures 15 K and 35 K. The current at 35 K minus the current at 15 K is plotted in fig. 4.9. When this difference is positive, the resistance of the Te D6 decreased with temperature and when it's negative, it means that the resistance of Te D6 increased with temperature. Hence, the gate voltage at which this plot crosses the X-axis will be close to the critical gate voltage. This crossing happens between 20 and 26 V, consistent with the previous result.

We also perfomed a gate scan at 25 K (fig. 4.8b). It being linear at and to some extent above 20 V shows that the device is still in the accumulation regime at these gate voltages. In this regime, the number of charge carriers, $N \propto |V_g - V_{Th}|$, where, V_g is the gate voltage.[45] The threshold voltage V_{Th} is given by the intercept you get by extending the linear region all the way to the X-axis. Here, it was 35.33±0.072 V.

By applying a current bias of 12 µA, we measured the voltage noise PSD of the device at different gate voltages. The spectra are plotted in fig. 4.10a. One of the features of electronic second order phase transitions is an increase in $1/f$ noise magnitude near the critical point.[16, 17] So, we plotted the inverse normalized noise PSD against frequency on a log-log plot and by fitting a line to it, we determined the $1/f$ noise magnitude, A, (fig. 4.10b)

$$\frac{V^2}{S_V(f)} = \frac{f}{A}$$

The $1/f$ noise magnitudes as a function of gate voltage are plotted in fig. 4.11. The $1/f$ noise magnitude changes with gate voltage. This is expected as both carrier number fluctuation as well

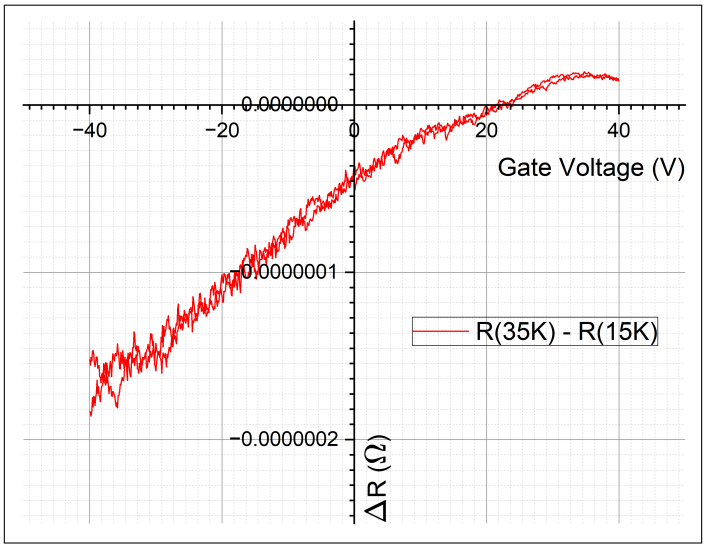

Figure 4.9: Difference in currents under a bias of 0.01 V at two different temperatures 15 K and 35 K for Tellurene D6.

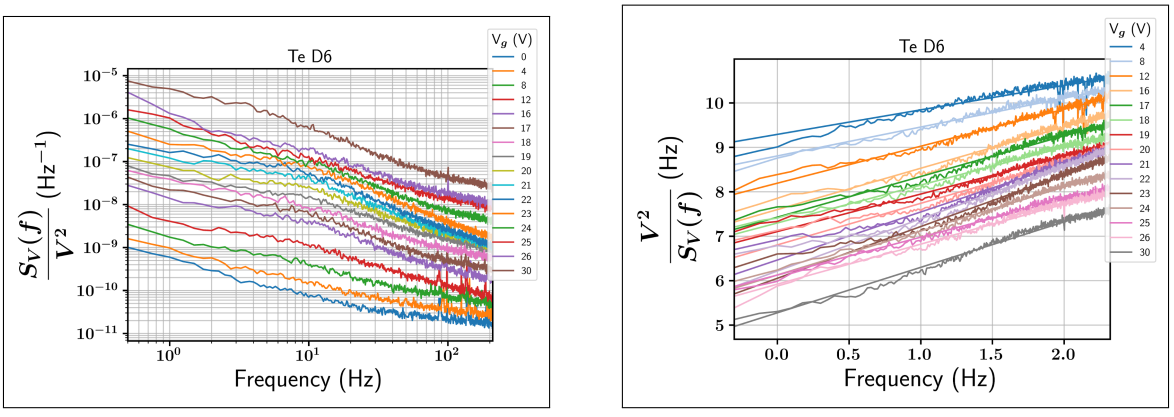

(a) (b)

Figure 4.10: (a) Voltage noise PSD of Tellurene D6 at 25 K at different gate voltages. (b) Normalized inverse noise PSD as a function of frequency at different gate voltages.

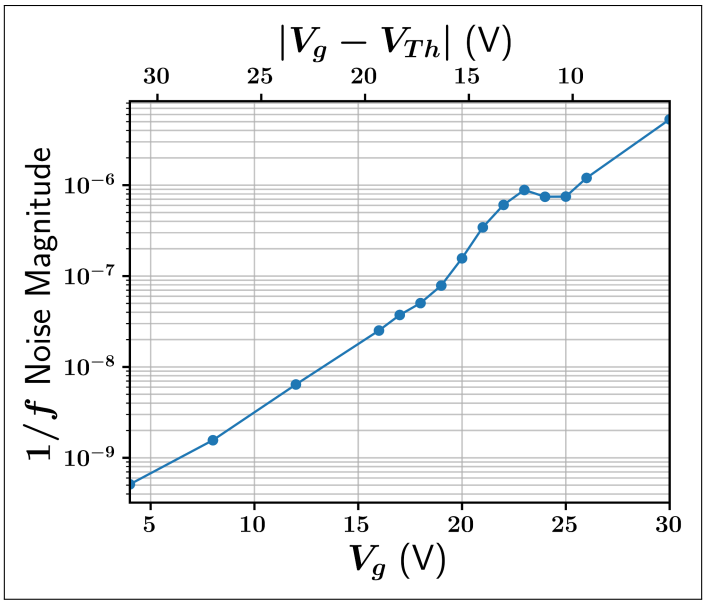

Figure 4.11: Normalized $1/f$ noise magnitude v/s gate voltage for Tellurene D6.

as mobility fluctuation models of $1/f$ noise predict that flicker noise magnitude will change with the number of charge carriers and hence the noise magnitudes at different gate voltages needs to be properly normalized before comparison. However, in our data, the noise magnitude increases with decreasing $|V_g - V_{Th}|$. The dependence also looks exponential since it appears to be approximately linear on a semilog plot. This is unexpected as the carrier number fluctuation model predicts that the $1/f$ noise increases linearly with $|V_g - V_{Th}|$ and the mobility fluctuation model predicts that the $1/f$ noise should increase proportional to $|V_g - V_{Th}|^2$.[45] Hence, we have been unable to normalize the PSDs at different gate voltages for proper comparison.

Chapter 5

Conclusions and outlook

The major contribution of this work is the successful implementation and validaton of a cross-correlation setup. By simulatneously acquiring two measurements of voltage or current time series and combining them, it becasme possible to measure power spectral density magnitudes even below the intrinsic noise floor of the amplifiers. This setup was validated by showing that the measured noise PSD magnitudes of metal film resistors show excellent agreement with theoretical predictions.

We also demonstrated that noise spectroscopy can be a useful probe of the microscopic processes occuring in nanodevices. By perfoming temperature-dependent noise spectroscopy on a CrSBr sample, we identified a generation-recombination process occuring in CrSBr and through rigorous data analysis, we calculated its activation energy to be 140 ± 1.2 meV. This process could be investigated further as a possible n-type doping process.

In our case, we were trying to characterized unintetional defects in CrSBr. However, when characterizing defects in other materials, it might be possible to do defect engineering. Concentrations of different defects can be controlled by methods like varying the ratios of different reagents during growth, plasma treatment, etc. In some cases, impurity atoms may also be intentionally doped. In such cases, systematic studies of the noise PSDs vs defect concentrations can make it possible to readily identify which generation-recombination processes are signatures of which defects.

Next, we tried to identify signatures of phase transition in noise PSDs of tellurne. Measurements at 220K revealed significant deviations from the conventional α exponent of $1/f$ noise. While these could indicated critical fluctuations, viewing the data in time domain revealed very slow generation-recombination processes as an alternative source behind the observed PSDs. This highlights the complexity in interpreting noise power spectral densities.

Our measurements also revealed some practical limitations of noise measurements. Firstly, there is always a constant 50 Hz interference from the environment in our noise data. Better sheilding can be achieved by putting all the measuring instruments and the cables connecting them

in a single, big metal box. This, together with maybe a better filtering technique could potentially reduce the 50 Hz hum further.

We also face a challenge with measuring voltage noise PSDs of large resistances due to the finiteness of the input impedances of our amplifiers. Amplifiers with higher input impedance can be used for measurements. However, they usually also have higher input voltage noise of their own. If increasing the input impedance of amplifiers is not possible, we could explore techniques to decrease the impedance of the devices. Applying a gate voltage and shining light on 2D materials can lead to generation of additional charge carriers and thus, lowering of resistance.

Another limitation of noise spectroscopy is that it requires long measurement times. Because 2D materials are especially susceptible to degradation with time, this poses a problem in getting consistent, reproducible results. Long measurement times create another problem in that multiple temperature sweeps are required, first to identify temperatures at which there are interesting features in the noise and then to measure the noise again in smaller temperature intervals. This repeated thermal cycling may also cause device degradation. Plus batteries used in amplifiers need to be charged between runs leading to extended downtimes.

Lastly, we note that we have been unable to obtain reproducible results. The possible reasons behind this may be that noise measurements are sensitive to the differing sample quality of the crystals and the variability in different devices or the degradation of the samples due to long measurement times and repeated thermal cycling. Correspondingly, it may be possible to make results more reproducible using better growth or fabrication techniques or by measures used to prolong the lifespan of 2D materials like surface passivation.[4]

Bibliography

[1] R. de-Picciotto, M. Reznikov, M. Heiblum, V. Umansky, G. Bunin, and D. Mahalu. *Direct Observation of a Fractional Charge*. In: Physica B: Condensed Matter **249–251** (June 17, 1998), pp. 395–400. ISSN: 0921-4526. DOI: 10.1016/S0921-4526(98)00139-2.

[2] L. Saminadayar, D. C. Glattli, Y. Jin, and B. Etienne. *Observation of the $e/3$ Fractionally Charged Laughlin Quasiparticle*. In: Physical Review Letters **79**.13 (Sept. 29, 1997), pp. 2526–2529. DOI: 10.1103/PhysRevLett.79.2526.

[3] Sh. Kogan. *Electronic Noise and Fluctuations in Solids*. 1st ed. USA: Cambridge University Press, June 2008. ISBN: 978-0-521-07019-5.

[4] S. Sarkar, A. Bid, K. L. Ganapathi, and S. Mohan. *Probing Defect States in Few-Layer MoS_2 by Conductance Fluctuation Spectroscopy*. In: Physical Review B **99**.24 (June 26, 2019), p. 245419. DOI: 10.1103/PhysRevB.99.245419.

[5] J. Müller. *Fluctuation Spectroscopy: A New Approach for Studying Low-Dimensional Molecular Metals*. 2011. DOI: 10.1002/cphc.201000814.

[6] M. A. Caloyannides. *Microcycle Spectral Estimates of 1/f Noise in Semiconductors*. In: Journal of Applied Physics **45**.1 (Jan. 1, 1974), pp. 307–316. ISSN: 0021-8979. DOI: 10.1063/1.1662977.

[7] F. Hooge. "1/f Noise Sources". In: *Advanced Experimental Methods For Noise Research in Nanoscale Electronic Devices*. Ed. by J. Sikula and M. Levinshtein. Dordrecht: Springer Netherlands, 2004, pp. 3–10. ISBN: 978-1-4020-2170-1. DOI: 10.1007/1-4020-2170-4_1.

[8] D. M. Fleetwood. *1/f Noise and Defects in Microelectronic Materials and Devices*. In: IEEE Transactions on Nuclear Science **62**.4 (Aug. 2015), pp. 1462–1486. ISSN: 1558-1578. DOI: 10.1109/TNS.2015.2405852.

[9] P. Dutta and P. M. Horn. *Low-Frequency Fluctuations in Solids: 1/f Noise*. In: Reviews of Modern Physics **53**.3 (July 1, 1981), pp. 497–516. ISSN: 0034-6861. DOI: 10.1103/RevModPhys.53.497.

[10] F. N. Hooge and L. K. J. Vandamme. *Lattice Scattering Causes 1/f Noise*. In: Physics Letters A **66**.4 (May 29, 1978), pp. 315–316. ISSN: 0375-9601. DOI: 10.1016/0375-9601(78)90249-9.

[11] T. MUSHA. *1/f Phonon-Number Fluctuations in Quartz Observed by Laser Light Scattering*. In: Phys. Rev. Lett. **64**.20 (1990), pp. 2394–2397.

[12] L. Ren and J. S. Liberis. *1/f-Noise in the Hall Voltage of Epitaxial n-GaAs*. In: Physica B: Condensed Matter **183**.1 (Jan. 1, 1993), pp. 40–44. ISSN: 0921-4526. DOI: 10.1016/0921-4526(93)90051-7.

[13] Z. Siwy and A. Fuliński. *Origin of $1/f^{\alpha}$ Noise in Membrane Channel Currents*. In: Physical Review Letters **89**.15 (Sept. 20, 2002), p. 158101. DOI: 10.1103/PhysRevLett.89.158101.

[14] R. F. Voss. *Evolution of Long-Range Fractal Correlations and 1/f Noise in DNA Base Sequences*. In: Physical Review Letters **68**.25 (June 22, 1992), pp. 3805–3808. DOI: 10.1103/PhysRevLett.68.3805.

[15] Y. Liu, P. Gopikrishnan, Cizeau, Meyer, Peng, and H. E. Stanley. *Statistical Properties of the Volatility of Price Fluctuations*. In: Physical Review E **60**.2 (Aug. 1, 1999), pp. 1390–1400. DOI: 10.1103/PhysRevE.60.1390.

[16] B. Hartmann. *Critical Slowing Down of the Charge Carrier Dynamics at the Mott Metal-Insulator Transition*. In: Physical Review Letters **114**.21 (2015). DOI: 10.1103/PhysRevLett.114.216403.

[17] S. Kalimuddin. *Exceptionally Slow, Long-Range, and Non-Gaussian Critical Fluctuations Dominate the Charge Density Wave Transition*. In: Physical Review Letters **132**.26 (2024). DOI: 10.1103/PhysRevLett.132.266504.

[18] D. S. Roy et al. *Signatures of Emergent Surface States across a Displacive Topological Phase Transition in Bi_4I_4*. Sept. 3, 2025. DOI: 10.48550/arXiv.2509.03469. arXiv: 2509.03469 [cond-mat]. Pre-published.

[19] G. Scandurra, C. Ciofi, J. Smulko, and H. Wen. *A Review of Design Approaches for the Implementation of Low-Frequency Noise Measurement Systems*. In: Review of Scientific Instruments **93**.11 (Nov. 21, 2022), p. 111101. ISSN: 0034-6748. DOI: 10.1063/5.0116589.

[20] G. Cannatà, G. Scandurra, and C. Ciofi. *An Ultralow Noise Preamplifier for Low Frequency Noise Measurements*. In: Review of Scientific Instruments **80**.11 (Nov. 9, 2009), p. 114702. ISSN: 0034-6748. DOI: 10.1063/1.3258197.

[21] M. Sampietro, L. Fasoli, and G. Ferrari. *Spectrum Analyzer with Noise Reduction by Cross-Correlation Technique on Two Channels*. In: Review of Scientific Instruments **70**.5 (May 1, 1999), pp. 2520–2525. ISSN: 0034-6748. DOI: 10.1063/1.1149785.

[22] G. Giusi, G. Scandurra, and C. Ciofi. *ESTIMATION ERRORS IN $1/f^{\gamma}$ NOISE SPECTRA WHEN EMPLOYING DFT SPECTRUM ANALYZERS*. In: Fluctuation and Noise Letters **12**.01 (Mar. 2013), p. 1350007. ISSN: 0219-4775. DOI: 10.1142/S0219477513500077.

[23] G. Scandurra and C. Ciofi. *Reducing Leakage Effects and Measurement Time in Low-frequency Noise Measurements*. In: Fluctuation and Noise Letters **24**.01 (Feb. 2025), p. 2440058. ISSN: 0219-4775. DOI: 10.1142/S0219477524400583.

[24] *Low Level Measurements Handbook*. 7th ed. Keithley Instruments. URL: https://download.tek.com/document/LowLevelHandbook_7Ed.pdf.

[25] T. Biktagirov, W. G. Schmidt, K. J. Schiller, M. Capra, J. E. Nitschke, L. Sternemann, M. S. Arndt, G. Zamborlini, A. Isaeva, and M. Cinchetti. *Intrinsic Defects as a Source of N-Type Conductivity in CrSBr*. In: npj 2D Materials and Applications **9**.1 (Dec. 3, 2025), p. 106. ISSN: 2397-7132. DOI: 10.1038/s41699-025-00640-7.

[26] K. Torres, A. Kuc, L. Maschio, T. Pham, K. Reidy, L. Dekanovsky, Z. Sofer, F. M. Ross, and J. Klein. *Probing Defects and Spin-Phonon Coupling in CrSBr via Resonant Raman Scattering*. In: Advanced Functional Materials **33**.12 (2023), p. 2211366. ISSN: 1616-3028. DOI: 10.1002/adfm.202211366.

[27] J. Klein et al. *Sensing the Local Magnetic Environment through Optically Active Defects in a Layered Magnetic Semiconductor*. In: ACS Nano **17**.1 (Jan. 10, 2023), pp. 288–299. ISSN: 1936-0851. DOI: 10.1021/acsnano.2c07655.

[28] M. Weile et al. *Defect Complexes in CrSBr Revealed Through Electron Microscopy and Deep Learning*. In: Physical Review X **15**.2 (June 4, 2025), p. 021080. DOI: 10.1103/PhysRevX.15.021080.

[29] J. Beck. *Über Chalkogenidhalogenide des Chroms Synthese, Kristallstruktur und Magnetismus von Chromsulfidbromid, CrSBr*. In: Zeitschrift für anorganische und allgemeine Chemie **585**.1 (1990), pp. 157–167. ISSN: 1521-3749. DOI: 10.1002/zaac.19905850118.

[30] M. K. Horton et al. *Accelerated Data-Driven Materials Science with the Materials Project*. In: Nature Materials **24**.10 (Oct. 2025), pp. 1522–1532. ISSN: 1476-4660. DOI: 10.1038/s41563-025-02272-0.

[31] A. Jain et al. *Commentary: The Materials Project: A Materials Genome Approach to Accelerating Materials Innovation*. In: APL Materials **1**.1 (July 18, 2013), p. 011002. ISSN: 2166-532X. DOI: 10.1063/1.4812323.

[32] K. Momma and F. Izumi. *VESTA 3 for Three-Dimensional Visualization of Crystal, Volumetric and Morphology Data*. In: Journal of Applied Crystallography **44**.6 (Dec. 1, 2011), pp. 1272–1276. ISSN: 0021-8898. DOI: 10.1107/S0021889811038970.

[33] C. Golz, Z. Galazka, A. Popp, S. B. Anooz, G. Wagner, F. Hatami, and W. T. Masselink. *Deep-Level Noise Characterization of MOVPE-grown β-Ga2O3*. In: Applied Physics Letters **115**.13 (Sept. 25, 2019), p. 133504. ISSN: 0003-6951. DOI: 10.1063/1.5098994.

[34] J. Klein et al. *Control of Structure and Spin Texture in the van Der Waals Layered Magnet CrSBr*. In: Nature Communications **13**.1 (Sept. 15, 2022), p. 5420. ISSN: 2041-1723. DOI: 10.1038/s41467-022-32737-8.

[35] N. R. Pradhan et al. *Metal to Insulator Quantum-Phase Transition in Few-Layered ReS2*. In: Nano Letters **15**.12 (Dec. 9, 2015), pp. 8377–8384. ISSN: 1530-6984. DOI: 10.1021/acs.nanolett.5b04100.

[36] B. H. Moon. *Metal-Insulator Transition in Two-Dimensional Transition Metal Dichalcogenides*. In: Emergent Materials **4**.4 (Aug. 1, 2021), pp. 989–998. ISSN: 2522-574X. DOI: 10.1007/s42247-021-00202-9.

[37] S. Lakhchaura, G. M. Anilkumar, and A. Rahman. *Carrier Density Induced Metal–Insulator Transition in Bi2O2Se Nanosheets*. In: ACS Applied Electronic Materials **7**.10 (May 27, 2025), pp. 4450–4456. DOI: 10.1021/acsaelm.5c00264.

[38] H. Tomlins. *Universal Transport at Lifshitz Metal-Insulator Transitions in Two Dimensions*. In: Physical Review Letters **135**.11 (2025). DOI: 10.1103/kc4r-72vj.

[39] V. Dobrosavljevic, N. Trivedi, and J. M. V. Jr. *Conductor Insulator Quantum Phase Transitions*. OUP Oxford, June 2012. 583 pp. ISBN: 978-0-19-959259-3. Google Books: NevADtUGXbsC.

[40] X. Ren, Y. Wang, Z. Xie, F. Xue, C. Leighton, and C. D. Frisbie. *Gate-Tuned Insulator–Metal Transition in Electrolyte-Gated Transistors Based on Tellurene*. In: Nano Letters **19**.7 (July 10, 2019), pp. 4738–4744. ISSN: 1530-6984. DOI: 10.1021/acs.nanolett.9b01827.

[41] P. Cherin and P. Unger. *Two-Dimensional Refinement of the Crystal Structure of Tellurium*. In: Acta Crystallographica **23**.4 (Oct. 10, 1967), pp. 670–671. ISSN: 0365-110X. DOI: 10.1107/S0365110X6700341X.

[42] C. Adenis, V. Langer, and O. Lindqvist. *Reinvestigation of the Structure of Tellurium*. In: Acta Crystallographica Section C: Crystal Structure Communications **45**.6 (June 15, 1989), pp. 941–942. ISSN: 0108-2701. DOI: 10.1107/S0108270188014453.

[43] W. Xie and C. D. Frisbie. *Electrolyte Gated Single-Crystal Organic Transistors to Examine Transport in the High Carrier Density Regime*. In: MRS Bulletin **38**.1 (Jan. 2013), pp. 43–50. ISSN: 0883-7694, 1938-1425. DOI: 10.1557/mrs.2012.310.

[44] R. Thangaraj. "Synthesis and Characterization of 2D Tellurene Flakes for Device Application". MA thesis. IISER Pune, May 2024.

[45] V. K. Sangwan, H. N. Arnold, D. Jariwala, T. J. Marks, L. J. Lauhon, and M. C. Hersam. *Low-Frequency Electronic Noise in Single-Layer MoS2 Transistors*. In: Nano Letters **13**.9 (Sept. 11, 2013), pp. 4351–4355. ISSN: 1530-6984. DOI: 10.1021/nl402150r.